Journal of Alloys and Compounds 794 (2019) 303–324

Contents lists available at ScienceDirect

Journal of Alloys and Compounds

journal homepage: http://www.elsevier.com/locate/jalcom

Review

Metal B-*N*-H hydrogen-storage compound: Development and perspectives

Kun Wang [a, b, **], Zuxiong Pan [b], Xuebin Yu [a, *]

[a] Department of Materials Science, Fudan University, Shanghai 200433, PR China
[b] Department of Chemistry, Anhui University, Hefei, Anhui 230601, PR China

ARTICLE INFO

Article history:
Received 16 February 2019
Received in revised form
20 April 2019
Accepted 23 April 2019
Available online 26 April 2019

Keywords:
Metal boron-nitrogen-hydrogen compound
Hydrogen storage material
Metal amidoborane
Metal hydrazinidoborane
Amine metal borohydrides

ABSTRACT

Metal boron-nitrogen-hydrogen (MBNH) compound is a kind of typical solid hydrogen storage material characterized by hydrogen-rich B-N species, which has been developed very fast in the last decade due to its high hydrogen capacity and the tunable hydrogen storage properties, such as metal amidoborane ($M(NH_2BH_3)_n$, MAB), metal hydrazinidoborane ($M(NH_2NH_2BH_3)_n$, MHB), amine metal borohydride ($M(BH_4)_n \cdot mNH_3$, AMB) and their derivatives. MAB is obtained by replacing a hydrogen cation of AB (NH_3BH_3) by a light metal cation (such as the alkali or alkali earth metal, generally), which was a famous hydrogen-storage material in last 15 years. MHB is formed by replacing a H(N) atom with light metal, which is similar with that of MAB. AMB is synthesized by the reaction between metal borohydrides and ammonia. There are a large amount of AMBs prepared in the recent ten years with different metals or different coordination numbers of NH_3. In this field, all the compounds are containing a strong Lewis acid/base interaction (such as B-N interaction). Hydrogen is generated from the dihydrogen bond of $H^{\delta+} \cdots H^{\delta-}$, where the metal works as a controllable hydrogen carrier to improve the purity of product in the dehydrogenation process. In this review, we focus on the novel solid MBNH compounds including MAB, MHB and AMB with their synthesis methods, structures and dehydrogenation properties. We hope this review can enlighten more extensive studies for the development of new MBNH compounds with advanced hydrogen storage performances.

Contents

* Corresponding author.
** Corresponding author. Department of Chemistry, Anhui University, Hefei, Anhui 230601, PR China.
E-mail addresses: wangkun@ahu.edu.cn (K. Wang), yuxuebin@fudan.edu.cn (X. Yu).

https://doi.org/10.1016/j.jallcom.2019.04.240
0925-8388/

1. Introduction

Hydrogen energy is a kind of sustainable and clean energy, which satisfies the global socioeconomic requirements. The generation of high purified hydrogen and the safe storage method are the central components for the application of hydrogen energy. Therefore, to improve the performances of present hydrogen storage materials, we should focus on the efficient producing, storage and delivering of hydrogen. The cyclic utilization of hydrogen storage material is also a key technical issue that should be overcome in the research. The target of DOE (US department of Energy) is to obtain the system-based hydrogen storage material with 40 g/l volumetric hydrogen density (g H_2/L system) before 2025 [1]. So there are tremendous efforts for researching the materials, which can not only hold sufficient hydrogen in terms of gravimetric and volumetric densities, but also possess suitable thermodynamic kinetic properties. In the last decades, different kinds of potential hydrogen storage media such as MOFs [2–4], carbon materials [5,6], metal hydrides [7–16] and chemical hydrides [17–22], have been attracted extensive investigations.

For B-*N*-H hydrogen storage materials, the hydrogen atom shows hydridic or protonic state normally [23]. The dehydrogenation proceeds after the formation of $H^{\delta+} \cdots H^{\delta-}$ bond [24]. Generally, after introducing metal cations, the dehydrogenation performances of MBNH systems are improved compared with the metal-free BNH system. In this review, we plan to describe the classic MBNH compounds in three sections: metal amidoborane (MAB), metal hydrazinidoborane (MHB) and amine metal borohydrides (AMB).

As a traditional Lewis acid/base adducts, ammonia borane (AB, NH_3BH_3) is a representative chemical hydrogen storage material, gained intensive attentions for the potential application. AB was first prepared in 1955 [25] with a high gravimetric storage density (up to 19.6 wt%), which appears nonflammable and nonexplosive properties under room temperature. The recent theoretical study proves that the formation of ammonia diborane ($H_3NBH_2(\mu\text{-}H)BH_3$) in the decomposition of AB leads to the release of NH_4^+, which in turn triggers an autocatalytic H_2 production cycle [26]. The standard enthalpy of the formation of AB is -59.97 ± 0.37 kcal/mol [27], suggesting that it is too stable to realize the reversible hydrogen absorption and desorption. MAB is commonly generated by metathesis between AB and metal hydrides. This part will be discussed in section 1.

As another high hydrogen content and less-toxic exhibition of hydrazine, MHB, prepared similar to that of MAB, can be possibility used as the propellant or additive for hybrid rockets [28]. It has been reported that MHB is more suitable to thermolytic dehydrogenation with improved properties in comparison to the parent

borane [29]. The latest study reveals that the $Ni_{0.6}Pt_{0.4}$/g-C_3N_4 nanosheets appears outstanding catalytic activity toward hydrogen generation from hydrous hydrazine (giving 100% H_2 selectivity with a high turnover frequency (TOF) value of 2194 h^{-1}) at 323 K [30]. The Ni/Ni_2P heterostructure also exhibits catalytic performance of H_2 generation from the hydrolysis of AB under ambient conditions [31]. The description about MHB including the synthesis and discussion is surveyed in section 2.

Since the study of $LiBH_4$ has been discovered as the hydrogen storage material in 2003 [32], a variety of metal borohydrides have been developed with excellent hydrogen storage properties and fascinating structure flexibilities [33]. The metal borohydrides can be easily coordinated with NH_3 to form $M(BH_4)_n \cdot nNH_3$ (AMB). As the family of metal boron-nitrogen-hydrogen compounds, AMBs have been developed very fast in recent ten years, which appear attractive performances and even potential reversibility in the decompositions. This part will be discussed in section 3.

2. Metal amidoborane and the derivatives

Metal amidoborane is characterized as high hydrogen content with moderate decomposition temperature. The decomposition of MAB shows more purified products than that of AB [34–36]. The common synthesis method of MAB is by ball milling the solid metal hydrides or metallic amino compounds (MH or MNH_2) with AB [37–39]. One hydrogen atom connected with N atom of AB is replaced in the process, where the hydrogen atom can be exchanged on the interface of the two solid compounds [40,41]. The synthesis reactions can be summarized as equations (1) and (2). The metal cation with larger electronegativity leads to more stable dihydrogen bond and better purity of released hydrogen [42,43]. The polarity of B-H, N-H or B-N bond can be tunable by introducing different metal cations [44].

$$\mathbf{MH_n + nNH_3BH_3 \rightarrow M(NH_2BH_3)_n + nH_2} \quad (1)$$

$$\mathbf{M(NH_2)_n + nNH_3BH_3 \rightarrow M(NH_2BH_3)_n + nNH_3} \quad (2)$$

2.1. Mono metal amidoborane and the derivatives

Fig. 1 summarizes mono metal amidoboranes and their derivatives, including their experimental crystal properties. The physical parameters including the syngony, crystal parameters and the dehydrogenation properties are listed in Table 1.

2.1.1. Alkali-metal (Li/Na/K) amidoborane and their derivates

2.1.1.1. Synthesis. Mayer et al. first reported the synthesis of $LiNH_2BH_3$ (LiAB) by the reaction of n-butyllithium and AB in THF solution at 0 °C [54]. Chen's group prepared LiAB by ball milling AB and LiH (or mixing them in THF solution) [35,45,55]. By tracking the process in the reaction, they summarized the pathway as reaction (3) [45]. The phase transition from α-LiAB to β-LiAB was also discussed in this research, where the crystal structures are listed in Table 1.

$$\mathbf{2LiH + 2AB \rightarrow LiH + LiNH_2BH_3 \cdot NH_3BH_3 + H_2 \rightarrow 2LiAB + H_2} \quad (3)$$

Monoammoniate of $LiNH_2BH_3 \cdot NH_3$ (LiAB NH_3) is one of the derivatives of LiAB, which was prepared by the coordination between LiAB and NH_3 under the room temperature [39]. It appears the amorphous phase in the normal condition. LiAB·NH_3 shows the reversibility of the deammoniation and ammonia absorption under the room temperature [39].

$LiNH_2BH_3 \cdot NH_3BH_3$ (LiAB·AB) can be prepared by ball-milling LiAB and AB with the molar ratio of 1:1 or LiH and AB with the ratio of 1:2 [42,46].

Schlesinger et al. first prepared $NaNH_2BH_3$ (NaAB) in 1938 from the reactants of B_2H_6-diethyl ether, ammonia and sodium under −77 °C [56]. The formed NaAB is the white powder, which is similar with that of LiAB. Until 2008, Chen's group synthesized NaAB by ball-milling NaH and AB as shown in equation (1). However, the synthesis in THF solution by mixing NaH (or $NaNH_2$) and AB results in the formation of NaAB-THF [57,58].

Mixing AB with Na or $NaNH_2$ in a refluxing tetrahydrofuran affords the new compound as $Na(BH_3\text{-}NH_2\text{-}BH_3)$ through the intermediate of NaAB in the process. The synthesis is showed as equation (4). The crystal of $Er(BH_3\text{-}NH_2\text{-}BH_3)Cl_2(THF)_3$ proves the structure of DADB is an ion pair of $[NH_4]^+[BH_3\text{-}NH_2\text{-}BH_3]^-$ [56].

$$\mathbf{4HNRR' \cdot BH_3 + 2Na \rightarrow 2Na(H_3B - NRR' - BH_3) + H_2 + 2HNRR'} \quad (4)$$

The study of Burrell et al. indicates that the reaction of AB in THF with 1 equiv. of KH for 4 h afforded KNH_2BH_3 (KAB) with the yield of 95%. The Van Der Waals interaction between K^+ and $[BH_3]$ groups supersedes the dihydrogen bonding in AB as the stabilizing factor of the crystal structure [47].

2.1.1.2. Decomposition. The decomposition temperature of LiAB is 92 °C by using TPD techniques, with the maximum decomposition rate at 108 °C. About 8 wt% of hydrogen is released from LiAB by volumetric-release measurement. No diborane has been detected in the decomposition process [35]. 2 equiv. H_2 can be released from LiAB in 19 h at 92 °C. Ryan pointed that the orthogonal motion of Li and B atoms triggers the dehydrogenation at low temperature by the method of inelastic neutron scattering [59].

In the inert gas (Ar), LiAB·NH_3 releases pure hydrogen mainly at 40–70 °C, while 3 equiv. (11.18 wt%) H_2 can be released with the catalysis of the coordinated NH_3 [39], indicating that ammonia is in favour of the dehydrogenation. There are two steps in the decomposition: 1) the departure of ammonia; 2) the continuous dehydrogenation [60] after the deammoniation. The dehydrogenation of LiAB·AB also includes two steps. It releases 6.0 wt% hydrogen (2 equiv.) at 57 °C and the extra 8.0 wt% hydrogen liberates (2.7 equiv.) at 228 °C. The process was summarized as equation (5) [61].

$$\mathbf{LiNH_2BH_3 \cdot NH_3BH_3\ (s) \xrightarrow{step1} [LiN_2B_2H_7](s) + 2H_2\ (g)}$$
$$\mathbf{\downarrow\ step2} \quad \mathbf{(5)}$$
$$\mathbf{LiN_2B_2H(s) + 3H_2\ (g)} \quad (5)$$

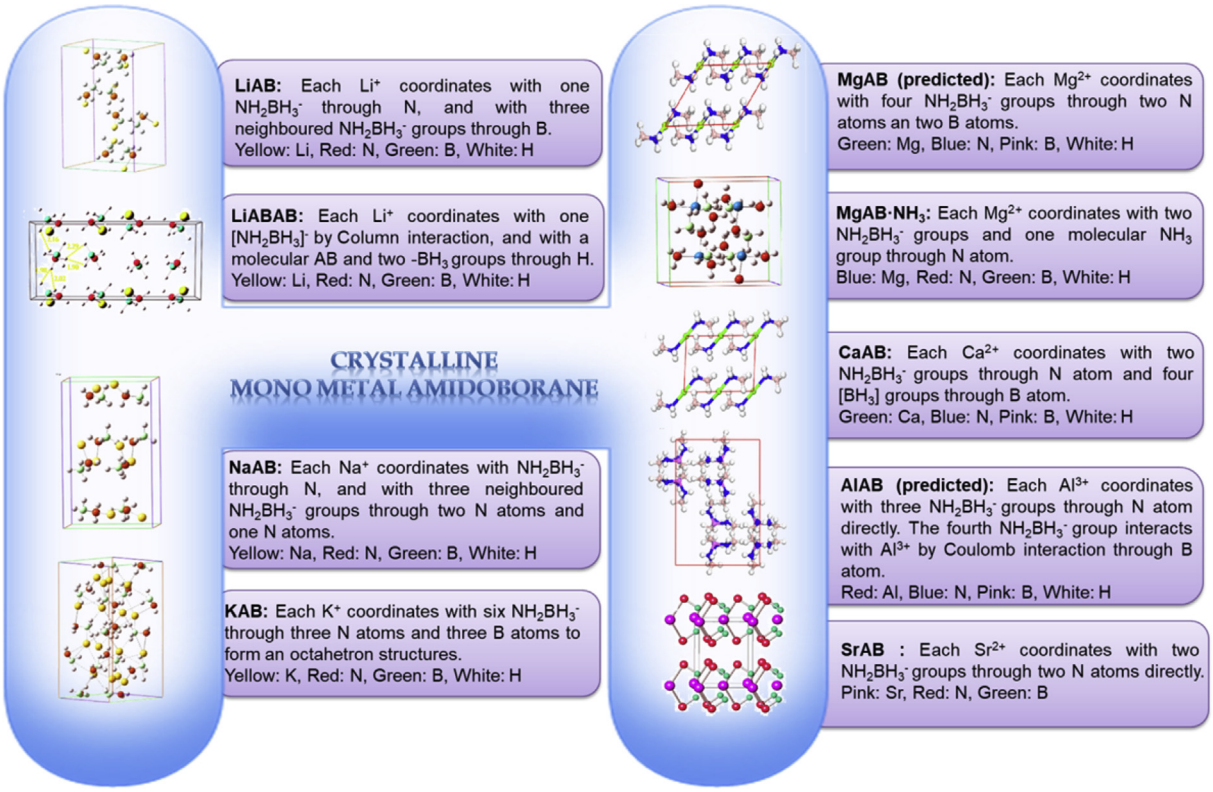

Fig. 1. The structure of crystalline mono metal amidoborane (MAB, M = Li/Na/K/Mg/Ca/Al/Sr).

Table 1
The syngony, groups, crystal parameters and the dehydrogenation properties of MAB and their derivatives.

Compound	Crystal parameters	Properties of decompostion	
		H content (wt %)	Initial T_{dec} (°C)
LiAB (α) [45]	*Orthorhombic* system; *Pbca* group; a = 7.133 Å, b = 13.949 Å, c = 5.150 Å	11	92
LiAB (β) [45]	*Orthorhombic* system; *Pbca* group; a = 15.146 Å, b = 7.720 Å, c = 9.268 Å	11	92
LiAB NH_3 [39]	*Orthorhombic* system; *Pbca* group; a = 9.711 Å, b = 8.703 Å, c = 7.200 Å	11.18	60
LiAB· AB [46]	*monoclinic* system; $P2_1/c$ group; a = 7.05 Å, b = 14.81 Å, c = 5.13 Å, β = 97.49°	14.3	50
NaAB [35]	*Orthorhombic* system; *Pbca* group; a = 7.469 Å, b = 14.655 Å, c = 5.653 Å	7.4	89
KAB [47]	*Orthorhombic* system; *Pbca* group; a = 9.430 Å, b = 8.261 Å, c = 17.34 Å	6.5	80
MgAB [48]	*monoclinic* system; *C2* group; a = 8.572 Å, b = 5.605 Å, c = 5.622 Å, β = 85.84°	10	104
MgAB NH_3 [48]	(Predicted) *monoclinic* system; $P2_1/a$ group; a = 8.882 Å, b = 8.947 Å, c = 8.070 Å, β = 94.07°	11.4	50
3MgAB·2NH_3 [49]	-	10.2	70
CaAB [42]	*monoclinic* system; *C2* group; a = 9.100 Å, b = 4.371 Å, c = 6.441 Å, β = 93.19°	3.6	90
CaAB NH_3 [50]	*monoclinic* system; $P2_1/c$ group; a = 10.583 Å, b = 7.369 Å, c = 10.201 Å, β = 120.8°	10.2	70
SrAB [51]	*monoclinic* system; *C2* group; a = 8.166 Å, b = 5.097 Å, c = 6.726 Å, β = 94.39°	13.47	93
AlAB [52]	(Predicted) *Orthorhombic* system; *Pbca* group; a = 17.151 Å, b = 7.562 Å, c = 12.387 Å	7	60
YAB [53]	*monoclinic* system; *C2/c* group; a = 13.189 Å, b = 7.822 Å, c = 14.874 Å, β = 92.426°	9.9 (with contamination)	50

NaAB melts at 57 °C and releases hydrogen up to 10.9 wt% at 200 °C (in total by TPD techniques and volumetric-release techniques). The dehydrogenation as a bimolecular reaction is catalyzed by Na^+ [62]. In the decomposition, the dimer structure of $[NH_3Na]^+[BH_3(NaNH)BH_3]^-$ leads to the liberation of ammonia at 55 °C [63]. The solid products of NaBNH is composited by $Na_{0.5}NBH_{0.5}$ and $(NaH)_{0.5}$ [64] as showed in equation (6).

$$\mathbf{NaNH_2BH_3 \rightarrow Na_{0.5}NBH_{0.5} + 0.5NaH + 2.0H_2} \quad (6)$$

KAB can evolve 6.5 wt% hydrogen at 80 °C. The decomposition process from 80 to 250 °C is composed from three stages: 1.5 equiv. hydrogen liberation at 80 °C, 0.5 equiv. hydrogen liberation at 80–160 °C and all the last hydrogen liberation from 160 °C to higher temperature. No ammonia is detected in the process. The decomposition of KAB follows the principle as: MAB→xMH + yM-N-B-H + $n$$H_2$ [65].

2.1.1.3. Theoretical analysis. As for LiAB, Shevlin et al. reported that the energy barrier of dehydrogenation through the intermediate of $[BH_4]^-[LiNHBH_2LiNH_2]^+$ is 0.13 eV (12.53 kJ/mol) lower than that of the pathway without the formation of the intermediate by first principle calculation [66]. Lee's calculation indicates that the energy barrier of the dehydrogenation is 1.57 eV (151.33 kJ/mol) by forming the transition structure of Li-H-H-Li by using the CCSD(T) method [67]. The similar calculation is reported by Kim et al. that the barrier is 1.46 eV (140.72 kJ/mol) through the transition state of triangle structure of Li-H-Li [68]. The direct formation of B-H···H-N intermolecularly requires the activation energy of 2.12 eV (204.35 kJ/mol) [68].

As for LiAB·AB, it releases hydrogen through the interface of LiAB and AB at lower temperature than pure AB or LiAB [69]. The formation of hydrogen bridge bond decreases the hydrogen barrier to 100 kJ/mol for the first dehydrogenation by using mp2 and CCSD(T) method [68].

2.1.2. $Mg(NH_2BH_3)_2$ (MgAB) and its ammonia coordinated derivatives

2.1.2.1. Synthesis. The first successful synthesis of MgAB is from the post-milled MgH_2/2AB or MgAB/2AB through the mobile phase of MgAB* under mild temperature (≤70 °C) [70]. There is a phase transition from AB to AB*. The particularity is caused by the weak deprotonation ability of Mg^{2+} [42,71]. The ammonia coordinated MgAB include $Mg(NH_2BH_3)_2\cdot nNH_3$ (MgAB·$n$$NH_3$) and 3 $Mg(NH_2BH_3)_2\cdot 2NH_3$ (3MgAB·$2NH_3$). $Mg(NH_2BH_3)_2\cdot 2NH_3$ can be prepared by ball-milling $Mg(NH_2)_2$ and AB with the ratio of 1:2. Then MgAB·NH_3 can be formed by removing 1 M NH_3 from $Mg(NH_2BH_3)_2\cdot 2NH_3$, which is the most stable compound of different MgAB·$n$$NH_3$ compounds [48]. Similarly, 3MgAB·$2NH_3$ is synthesized by ball-milling AB and Mg_3N_2 with the ratio of 6:1 directly [49].

2.1.2.2. Decomposition. MgAB is a stable compound at room temperature and can release ~10 wt % hydrogen with high purity upon heating the sample to 300 °C [70]. MgAB·NH_3 starts to decompose at 50 °C, where the peak temperature is between 74 and 300 °C with slight ammonia contamination. Totally 11.4 wt% hydrogen is liberated by heating MgAB to 300 °C [48]. The dihydrogen bond is formed by the neighbored NH_3 and BH_3 groups. As for 3MgAB·$2NH_3$, the coordinated ammonia affects the dehydrogenation process. It releases 1.6 wt% hydrogen at 70 °C. There is 11 wt % hydrogen liberated at 300 °C in 1 h [49]. The final product is the mixture containing BN_3 and HBN_2.

2.1.3. $Ca(NH_2BH_3)_2$ (CaAB) and its ammonia coordinated derivatives

2.1.3.1. Synthesis. CaAB was first prepared by the reaction between AB and CaH_2 in THF [34]. Another method is by ball-milling the mixture of CaH_2 and 2AB [42]. Similar with the synthesis of MgAB·NH_3, CaAB·$2NH_3$ is synthesized by AB and $Ca(NH_2)_2$ with the ratio of 2:1 directly [72,73]. Then CaAB·NH_3 is formed by removing 1 M of ammonia from CaAB·$2NH_3$ [50].

2.1.3.2. Decomposition. CaAB starts to release hydrogen at 70 °C, where the most significant mass loss appears is at 120 °C by the thermogravimetric analysis. The hydrogen liberation ends at 245 °C with a total of 4 equiv. hydrogen. The decomposition of CaAB·NH_3 mainly releases ammonia below 100 °C. However, 10.2 wt% hydrogen is released when heating the sample in the temperature range from 100 to 300 °C with the contamination of ammonia less than 0.1 wt%. The main product is composed by CaB_2N_3H [50].

2.1.3.3. Theoretical analysis. The alkalinity of $H^{\delta-}$ in CaH_2 is strong enough to deprotonate AB to form CaAB, which is different from that of MgH_2 [42,74]. The band gap of crystal CaAB is 6.12 eV (589.90 kJ/mol) by using GW approximation [75]. In CaAB·NH_3, ammonia catalyzes the intermolecular dehydrogenation between NH_3 and H(B) by activating the proton of AB. Besides the coordinated NH_3, the central metal of Ca^{2+} suppresses the liberation of ammonia. Therefore, CaAB·NH_3 appears improved dehydrogenation properties compared with that of CaAB [76,77].

2.1.4. $Sr(NH_2BH_3)_2$ (SrAB) $Y(NH_2BH_3)_3$ (YAB), $Al(NH_2BH_3)_3$ (AlAB) and their derivatives

2.1.4.1. Synthesis. SrAB is prepared by ball-milling SrH_2 and AB with the ratio of 1:2 [51]. AlAB can be prepared by mixed AB and $AlCl_3$. The crystal structure of AlAB has not been reported by now [78]. Caused by the electron deficiency of Al^{3+}, there is a derivative composed as $[Al(NH_2BH_3)_6^{3-}][Al(NH_3)_6^{3+}]$, which is synthesized by ball milling (150 rpm for 2 h) $AlH_3\cdot OEt_2$ with liquid $NH_3BH_3\cdot nNH_3$ (n = 1–6) with the ratio of 1:3 under ammonia atmosphere at 0 °C with the productivity is 95% [79]. YAB is synthesized by ball-milling YCl_3 with LiAB in the molar ratio of 1:3. However, it's difficult to separate YAB and YCl_3 by using this method [53,80].

2.1.4.2. Decomposition. SrAB starts to decompose at 60 °C and 6 wt % hydrogen is released in the decomposition until 200 °C, with the byproducts of ammonia and diborane (5.2 wt%) in the process [51]. AlAB starts to decompose at 60 °C and ammonia can be detected at 80 °C [81,82]. $[Al(NH_2BH_3)_6^{3-}][Al(NH_3)_6^{3+}]$ begins to release hydrogen at 65 °C and a total of 10.3 wt% (8.6 equiv.) hydrogen is released upon heating to 105 °C [79]. YAB is thermodynamically unstable under ambient conditions. A fresh prepared YAB decomposes large amounts of H_2 but with a noticeable ammonia impurity from 50 to 250 °C in argon gas [53].

2.2. Multi metal amidoborane (MM'AB)

Different from the mono-metallic amidoborane, two or more metal centers of MM'AB (multi metal amidoborane) always improve the hydrogen purity in the decomposition, because both of them suppress the liberation of ammonia and diborane at the meantime [83,84]. In this part, we summarized the development of MM'AB in recent ten years. The structural parameters and hydrogen-storage properties are listed in Table 2. The typical bond lengths of MM'AB are listed in Table 3. The crystal structures of MM'AB are showed in Fig. 2.

2.2.1. Na-$M(NH_2BH_3)_n$ (M = Li, Mg, Al)

2.2.1.1. Synthesis. $NaLi(NH_2BH_3)_2$ (SLAB) can be obtained by disk milling of dry LiH, NaH and AB with the ratio of 1:1:2, where the reaction is showed as equation (7). The substrates were milled three times for 3 min with two 5 min breaks in the synthesis process [85].

$$\mathbf{NaH + LiH + 2NH_3BH_3 \rightarrow NaLi(NH_2BH_3)_2 + 2H_2} \quad (7)$$

The wet chemical method was also successful in the synthesis of SLAB by dissolving the mixture of LiAB and NaAB in THF with the ratio of 1:1 as showed in equation (8) [92].

Table 2
The syngony, groups, crystal parameters and the dehydrogenation properties of MM'AB.

Compound	Crystal structure	Properties of decompostion	
		H content (wt %)	Initial Tdec (°C)
SLAB [85]	*Triclinic* system; *P1* group; a = 5.020 Å, b = 7.120 Å, c = 8.920 Å α = 103.003°, β = 102.200°, γ = 103.575°	9.0	58
SMAB [86]	*Monoclinic* system; *P21* group; a = 17.011 Å, b = 9.432 Å, c = 9.398 Å, β = 115.99°	7.4	50
DSMAB [87]	*Orthorhombic* system; $I4_1/a$ group; a = 9.415 Å, b = 9.415 Å, c = 12.413 Å	8.4	65
SAAB [88]	*Triclinic* system; *P1* group; a = 9.435 Å, b = 7.720 Å, c = 7.762 Å α = 97.211°, β = 109.223°, γ = 89.728°.	9.0	71
PAAB [89]	*Triclinic* system; *P1* group; a = 9.715 Å, b = 7.822 Å, c = 7.875 Å α = 95.358°, β = 109.944°, γ = 89.629°.	6.0	92
DPMAB [90] [a]	*Tetragonal* system; $I4_1/a$ group; a = 9.597 Å, b = 9.597 Å, c = 13.581 Å, β = 120.98°	7.0	50
LCA2B3 [91]	(Proposed parameters) *Monoclinic* system; a = 7.302 Å, b = 12.551 Å, c = 5.059 Å	7.9	50

[a] The structure and properties are based on the study of post milled DPMAB + $Mg(NH_2)_2$.

Table 3
The reported typical bond length (Å) of MM'AB.

	B-H	N-H	M-N	M′-B	B-N
SLAB [85]	1.22–1.32	1.00–1.10	(Li-N): 2.157/2.161/2.261	(Li-B) 1.875 (Na-B): 2.199–2.513	1.51–1.61
SMAB (predicted) [86]	1.23	1.04	(Mg-N): 2.12	(Na-B): 2.77/2.92	1.58
DSMAB [87]	1.27	1.03	(Mg-N): 2.11	(Na-B): 2.90–3.63	1.56
SAAB (Calculated) [88]	–	–	(Al-N): 1.90	(Na-B): 2.92–3.55	–
PAAB [89]	–	–	(Al-N): 1.838–1.909	(K-B): 3.131–3.602	–
DPMAB [90]	1.24[a]	1.04[a]	(Mg-N): 2.12	(K-B): 3.36/3.43	1.57[a]

[a] The parameters are from the calculations in Ref. [83].

$$\mathbf{NaNH_2BH_3 + LiNH_2BH_3 \longrightarrow NaLi(NH_2BH_3)_2} \quad (8)$$

As showed in equation (9), $NaMg(NH_2BH_3)_3$ (SMAB) was prepared by mechanically milling the 3AB and $NaMgH_3$ powder mixture at 45 °C overnight. The combination of Na^+ and Mg^{2+} tunes the reactivities of the reactants [86].

$$\mathbf{3NH_3BH_3 + NaMgH_3 \rightarrow NaMg(NH_2BH_3)_3 + 3H_2} \quad (9)$$

$NaMg(NH_2BH_3)_3$ (DSMAB) is the first example of the mixed-metal amidoborane, which was synthesized by ball milling of NaH, MgH_2 and AB under 1 bar He directly [87] (as equation (10)).

$$\mathbf{2NaH + MgH_2 + 4NH_3BH_3 \rightarrow Na_2Mg(NH_2BH_3)_4 + 4H_2} \quad (10)$$

$NaAl(NH_2BH_3)_4$ (SAAB) is the first Al-based amidoborane, which was obtained through a mechanochemical treatment of $NaAlH_4$ and 4AB after 240 milling/break cycles of 3/5 min. The hydrogen productivity of SAAB is 90%. Totally 4.5 wt% pure hydrogen can be obtained in the synthesis process (equation (11)) [88].

$$\mathbf{NaAlH_4 + 4NH_3BH_3 \rightarrow NaAl(NH_2BH_3)_4 + 4H_2} \quad (11)$$

2.2.1.2. Decomposition. There are two steps in the decomposition of SLAB, one is the step in 75–110 °C (with 6.0 wt % mass loss), the other one is the step in 130–200 °C (with another 3.0 wt % mass loss). About 1/5 hydrogen content is still remained in the amorphous solid when completing thermal decomposition [85]. SMAB starts to release hydrogen from around 50 °C and releases 7.4 wt% (about 5 equiv.) of hydrogen until 250 °C with the solid residue of $NaMgB_3N_3H_5$ [86]. However, DSMAB releases 8.4 wt % pure hydrogen from 65 °C. Minimal ammonia and borane contamination has been detected after 400 °C [87]. As for SAAB, it releases 9 wt % of pure hydrogen in two steps with the peaks (the most significant mass loss) at 120 and 160 °C. And the simplified total decomposition reaction is summarized as equation (12) [88].

$$\mathbf{NaAl(NH_2BH_3)_4 \rightarrow NaAlH_4 + AlN_4B_3H_{(0-3.6)} + (6.2 - 8.0)H_2} \quad (12)$$

2.2.1.3. Theoretical analysis. In SLAB, Li^+ stabilizes the entire structure while Na^+ acts as a counterpart, which transfers hydrogen anion to form a dihydrogen bond through an intramolecular oligomer of $[NH_2BH_2NH_2BH_3]^-$ [93]. As for SMAB, the band gap of SMAB is 4.4 eV (424.12 kJ/mol) based on the optimization [83]. Mg^{2+} as the stronger Lewis acid dominates the symmetry and stabilizes the structure. Li^+ as a counterpart, which is a weaker Lewis acid controls the motion of N and B [94]. In DSMAB, Mg^{2+} stabilizes the tetrahedron structure with sp^3 hybridization. The energy barrier of the determining step in the dehydrogenation is 242.40 kJ/mol, which is consistent with the experiment [95]. The calculation indicates that DSMAB is the compound with a large band gap of 5.0 eV (481.95 kJ/mol).

2.2.2. $K\text{-}M(NH_2BH_3)_n$ (M = Mg, Al)

2.2.2.1. Synthesis. $K_2Mg(NH_2BH_3)_4$ (DPMAB) prepared by ball milling $MgAB\cdot NH_3$ and KH with the molar ratio of 1:1 under Ar atmosphere at 200 rpm for 10 h (equation (13)). There is 1 equiv. of hydrogen and a detectable amount of ammonia (3 wt%) released in the synthesis process [90].

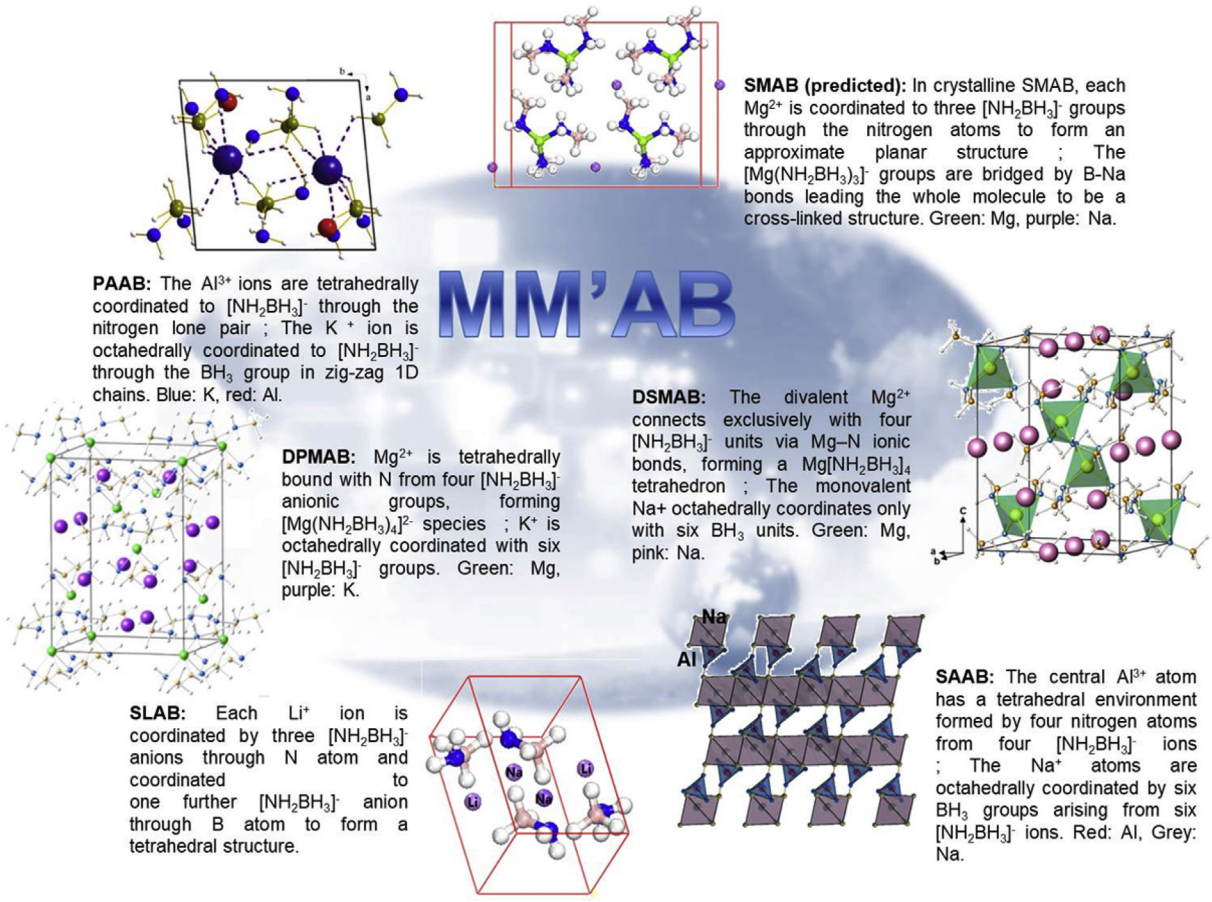

Fig. 2. The coordination pathway of multi metal amidoborane.

$$\mathbf{2KH + 2Mg(NH_3BH_3).NH_3 \rightarrow K_2Mg(NH_2BH_3)_4 + Mg(NH_2)_2 + 2H_2} \quad (13)$$

$KAl(NH_2BH_3)_4$ (PAAB) is prepared by ball milling $KAlH_4$ and 4AB with 120 cycles for10 h (5 min milling and 2 min break in one cycle). The hydrogen productivity is 91 wt % for PAAB [89].

2.2.2.2. Decomposition. In DPMAB, hydrogen is released above 147 °C, with the peak temperature of 158 °C by using TG-DSC and TPD-MS methods. A total of 7 wt% (~9.7 equiv.) of hydrogen was obtained upon raising temperature to 285 °C in the mixture of DPMAB and $Mg(NH_2)_2$ [90].

There are two exothermic steps from 92 °C (T_{peak} = 104 °C) and from 139 °C (T_{peak} = 153 °C) in PAAB's decomposition process by using TGA, DSC and MS analysis. A total of 6.0 wt% of hydrogen is observed at 262 °C. A tiny amount of NH_3, $N_3B_3H_6$ and B_2H_6 is observed in the decomposition [89].

2.2.2.3. Theoretical analysis. Structural study indicates that the band gap of DPMAB is 4.8 eV (462.67 kJ/mol), where the valence electrons of K is closed to the Fermi level in the valence band, which are excited firstly in the reaction. The weaker bond strength of B-H than that of N-H, which makes the first splitting of B-H bond in the dehydrogenation [83].

2.2.3. $LiCa(NH_2)_3(BH_3)_2$ (LCA_2B_3)

2.2.3.1. Synthesis. LCA_2B_3 is prepared by ball-milling CaAB and $LiNH_2$ with the ratio of 1:1 at 200 rpm for 5 h. Approximately 0.6 equiv. of hydrogen is released during the process as showed in equation (14) [91].

$$\mathbf{Ca(NH_2BH_3)_2 + LiNH_2 \rightarrow LiCa(NH_2)_3(BH_3)_2} \quad (14)$$

2.2.3.2. Decomposition. LCA_2B_3 starts to release hydrogen at 50 °C (T_{peak} = 135 °C). About 4.8 equiv. (7.9 wt%) hydrogen is released from the sample when heating the system to 500 °C. The decomposition process is proposed as equation (15).

$$\mathbf{LiCa(NH_2)_3(BH_3)_2 \rightarrow LiCa(N_2B)_3Li_3BN_2 + BN + H_2} \quad (15)$$

2.3. Summary

Most of the synthesis processes of MAB are based on the mechanic methods between a metal hydrides (or metal amides) and AB directly. The successful synthesis depends on the interaction between the Lewis acid (metal cations) and Lewis base (N atom in AB). There are lots of factors that affect the hydrogen productivity of MAB including the acidity, temperature, and conditions of reaction which have been discussed upside. There are also many analysis about the mechanisms of their dehydrogenation, where the metal as the hydrogen carrier for carrying $H^{\delta+}$ from N to form dihydrogen bond with $^{\delta-}H(B)$ [18,96,97]. As for the dehydrogenation properties, we summarized as in Table 4 for both mono-MABs and multi-MM'ABs.

The performance in the decomposition of MAB is controlled by

Table 4
The dehydrogenation properties of MAB and MM'AB.

Compound	Radius of center cations (Å)	Electronegativity of center cations	H content (Theor wt%)	H content (Exp wt% with the Temp)	Byproducts
LiAB [45]	0.76	14.59	13.61 wt%	10.9 wt% (90 °C)	ammonia (slightly)
LiAB·NH_3 [39]	0.76	14.59	14.88 wt%	11.18 wt% (60 °C)	ammonia (slightly)
LiAB·AB [46]	0.76	14.59	16.28 wt%	14 wt% (140 °C)	ammonia
NaAB [35]	1.02	9.44	9.47 wt%	7.5 wt% (90 °C)	ammonia (slightly)
$Na(BH_3NH_2BH_3)$ [56]	1.02	9.44	12.01 wt%	–	–
KAB [47]	1.38	6.47	7.26 wt%	6.5 wt% (80 °C)	None
MgAB [48]	0.72	17.13	11.91 wt%	10 wt% (300 °C)	None (300 °C)
MgAB·NH_3 [48]	0.72	17.13	12.88 wt%	11.4 wt% (300 °C)	ammonia (slightly)
3MgAB·2 NH_3 [49]	0.72	17.13	12.60 wt%	11 wt% (300 °C)	ammonia
CaAB [42]	1.00	11.30	10.03 wt%	9.0 wt% (500 °C)	ammonia (slightly)
CaAB·2NH_3 [50]	1.00	11.30	11.97 wt%	10.2 wt% (300 °C)	ammonia (slightly)
SrAB [51]	1.18	9.83	6.79 wt%	9.9 wt% (200 °C)	ammonia and diborane
AlAB [52]	0.54	26.72	12.89 wt%	10.3 wt% (190 °C)	ammonia (>100 °C)
$[Al(NH_2BH_3)_6^{3-}]$ $[Al(NH_3)_6^{3+}]$ [79]	0.54	26.72	15.15 wt%	10.3 wt% (105 °C)	ammonia
YAB [53]	0.9	14.82(III)	8.27 wt%	4 wt% (>130 °C)	ammonia
SLAB [85]	Na/Li: 1.02/0.76	Na/Li: 9.44/14.59	11.17 wt%	9.0 wt% (200 °C)	ammonia
SMAB [86]	Na/Mg: 1.02/0.72	Na/Mg: 9.44/17.13	10.97 wt%	7.4 wt% (250 °C)	ammonia
DSMAB [87]	Na/Mg: 1.02/0.72	Na/Mg: 9.44/17.13	10.55 wt%	7.8 wt% (285 °C)	ammonia & borazine (very slightly)
SAAB [88]	Na/Al: 1.02/0.54	Na/Al: 9.44/26.72	11.82 wt%	9 wt% (160 °C)	None
PAAB [89]	K/Al: 1.38/0.54	K/Al: 6.47/26.72	10.80 wt%	6 wt% (262 °C)	ammonia and diborane (slightly)
DPMAB [90]	K/Mg: 1.38/0.72	K/Mg: 6.47/17.13	9.04 wt%	7 wt% (285 °C)	NH_3, $N_3B_3H_6$ and B_2H_6 (slightly)
LCA_2B_3 [91]	Li/Ca: 0.76/1.00	Li/Ca: 14.59/11.30	9.78 wt%	7.9 wt% (500 °C)	None

the polarity of center metal. On the basis of Fajan's role, more active metal atoms lead to the better role in the hydrogen transferring process, which should appear large radius of ions and low electronegativity such as LiAB, NaAB and KAB. However, the metal cation with small radius and high electronegativity (high polarity) is difficult to form M – H bond caused by its covalence character, such as Al/Y-compounds. In the ammonia coordinated MAB, First-principle calculation show that [NH_3] molecules play crucial role as both activator for the break-up of B-H bond and supplier of protic H for the establishment of dihydrogen bonding [98]. On the basis of the calculation of the multi metal MM'AB, we presume that the primary cation is a kind of stronger Lewis acid such as Mg in SMAB or DSMAB, which are more possible to be the center to dominate the symmetry and space group, as well as stabilizing the structure in bimetallic amidoborane. The secondary cation, such as Li^+ or Na^+, as a weak Lewis acid with large ion radius and lower polarizing ability plays as a compensation role [83,99].

3. Metal hydrazinidoboranes (MHB)

As a kind of boron- and nitrogen-containing hydrogen-storage material, hydrazine borane (HB) also attracts many investigations due to its high gravimetric hydrogen densities (15.4 wt%) and the classic dihydrogen bond. The full dehydrogenation process of HB proceeds suitable in aqueous solution. Hydrazine borane shows a gradual pressure-induced decrease of its unit cell dimension and the process is reversible when the applied pressure is released [100]. Similar with AB, the dehydrogenation properties can be improved by introducing the alkali or alkali-earth metals into pristine HB, such as Li, Na, K, Mg and Ca. The crystal parameters and dehydrogenation characters are listed in Table 5. The crystal structures of MHB with their typical bond lengths are showed in Fig. 3.

3.1. $NH_2NH_2BH_3$ (HB)

3.1.1. Synthesis

Hydrazine borane (HB) can be prepared by the reaction of $NaBH_4$ and $(N_2H_5)SO_4$ in dioxane at around 30 °C for 3 days, with the yield of 80.3% and a product purity of 99.6% [101]. The heat for the formation of solid state HB is 42.7 ± 0.4 kJ/mol.

3.1.2. Decomposition

HB melts at around 60 °C with an enthalpy of 15 kJ/mol. It

Table 5
The syngony, groups, crystal parameters and the dehydrogenation properties of MM'AB.

Compound	Crystal structure	Properties of decompostion	
		H content (wt %)	Initial T_{dec} (°C)
HB [101]	*monoclinic* system; *P21/n* group; a = 8.258 Å, b = 8.221 Å, c = 10.372 Å, β = 94.95°.	11.9	60
LiHB [102]	*monoclinic* system; $P2_1/c$ group; a = 5.852 Å, b = 7.465 Å, c = 8.897 Å, β = 122.381°	11.69	<70
LiHB·2HB [102]	*monoclinic* system; $P2_1/c$ group; a = 8.149 Å, b = 8.960 Å, c = 14.972 Å, β = 116.091°	11.5	~70
NaHB [103]	*monoclinic* system; *P21/n* group; a = 4.974 Å, b = 7.958 Å, c = 9.292 Å, β = 93.814°	7.6	<60
KHB [104]	*monoclinic* system; *P21* group; a = 6.708 Å, b = 5.882 Å, c = 5.765 Å, β = 108.268°	7.3	~50

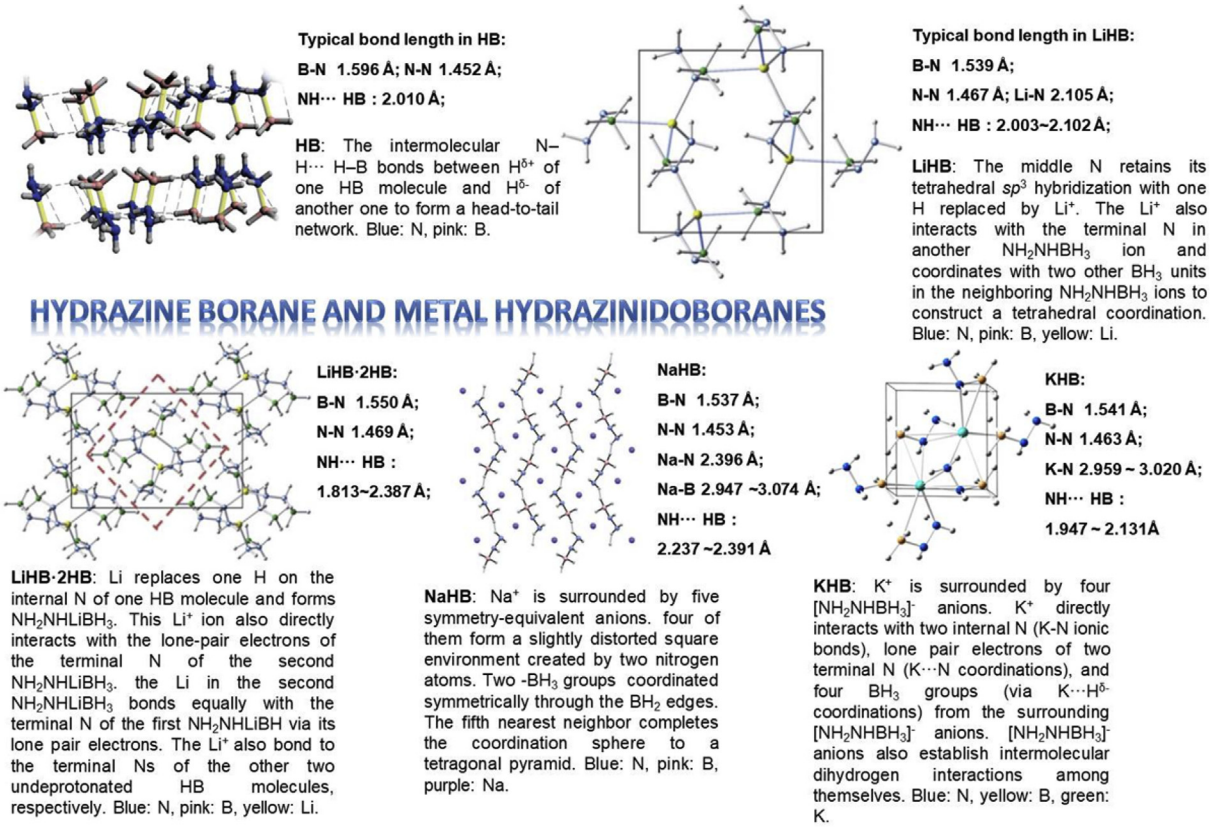

Fig. 3. Crystal structures of HB and MHB with the typical bond lengths (Å).

releases 28.7 wt% N_2H_4 at 105–160 °C. There are 2 equiv. hydrogen and shock-sensitive solid residue generated when heating the sample to 250 °C [101]. The decomposition can be summarized as: $N_2H_4BH_3 \rightarrow NBH + 2H_2 + 1/2\ N_2H_4$ [105].

3.1.3. Theoretical analysis

It is a weak charge donation of about 0.5 e from Lewis base to acid. There is no charge transfer intermolecularly within the crystal environment [106].

3.2. $M(NHNH_2BH_3)$ ($M = Li, Na, K$) and their derivatives

3.2.1. Synthesis

$Li(NHNH_2BH_3)$ (LiHB) is synthesized by ball milling (at 200 rpm) LiH and HB with the ratio of 1:1 under 1 bar He for 1–3 h [102]. The strong Lewis base $H^{\delta-}$ of LiH reacts with the protic hydrogen $H^{\delta+}$ on the middle NH_2 group of HB in the formation of LiHB [107]. The hydrazine borane adduct LiHB, $Li(NHNH_2BH_3)\cdot 2NH_2NH_2BH_3$ (LiHB·2HB) is generated after ball-milling 3HB-LiH mixture under 1 bar He at 200 rpm for 1–3 h [102]. Increasing the amount of LiH in the reactants does not replace more hydrogen atoms of HB. $Na(NHNH_2BH_3)$ (NaHB) is synthesized by ball milling HB and NaH with the ratio of 1:1 at −30 °C under argon atmosphere (250 rpm for tem minutes) [103]. Similarly, caused by the extreme active reactivity between dry KH and HB, the two reactants are stirred at 300 rpm within THF in an autoclave reactor for the generation of $K(NHNH_2BH_3)$ (KHB) [104].

3.2.2. Decomposition

LiHB starts to release hydrogen below 70 °C. There are 3 equiv. H_2 between 100 and 200 °C with the liberation of a minor amount of N_2 (0.7 mass%) and NH_3 (0.1 mass%) [102]. LiHB·2HB starts to dehydrogenate around 70 °C. Totally there is 11.5 wt% hydrogen at the range of 50–400 °C with the liberation of 8.9 wt% N_2 at 180–400 °C [102]. NaHB starts to liberate hydrogen below 60 °C with the solid melting. It loses 6 wt% H_2 at 60–100 °C. Totally there are 7.6 wt% hydrogen liberated until heating the sample to 150 °C. KHB releases hydrogen at around 50 °C. There is 7.3 wt% hydrogen liberated at 180 °C with a small amount of ammonia [104].

3.2.3. Theoretical analysis

The crystal LiHB is stabilized by the intermolecular $H^{\delta+} \ldots H^{\delta-}$ interaction. The length of B-N bond is shorter than that of pristine HB due to the strong electron detonation from N to Li^+ [102]. The dehydrogenation is started from the formation of the dimer structure of $NH_2NH(M)BH_2$-$NHNH(M)BH_3$ and $NH_2NH(M)BH{=}NNH(M)BH_3$ after the intermolecular interaction of $H^{\delta+}$ and $H^{\delta-}$, where M represents Li, Na and K [104].

3.3. Metal hydrides-hydrizine borane

3.3.1. Synthesis

Three mixtures (MgH_2-HB, CaH_2-HB and AlH_3-HB) are prepared by varying the milling conditions at 200–450 rpm with the ratio of 1:1 (1–18 cycles) in 10–30 min under argon atmosphere. They are only homogeneous binary mixtures of MH_x-HB without cation substitution in HB under this condition [108].

3.3.2. Decomposition

MgH_2-HB slowly evolves hydrogen from 40 °C. The accompanied liberation of NH_3, N_2 and N_2H_4 is observed from 60 to 120 °C in the decomposition. CaH_2-HB releases hydrogen below 60 °C. There

is 18.6 wt% weight loss from 25 to 400 °C including the contamination of NH_3 and N_2H_4. AlH_3-HB liberates hydrogen over the range of 50–270 °C with the byproduct of NH_3, N_2, N_2H_4 and B_2H_6. The dehydrogenation is between the $H^{\delta-}$ of MH_x and $H^{\delta+}$ of HB [108].

3.4. Summary

Similar with MAB, most of MHBs are synthesized by mechanically milling. Although it is not suitable to use pristine HB as a solid-state hydrogen storage material caused by its high decomposition temperature and shock-sensitive products, the development of HB as the intermediate to closed the hydrogen cycle is still under investigation [28,109]. The unsolved problem is to identify the components of the corresponding thermal residues after decomposition, which is the bottleneck problem to realize the recyclability of MHB. All the decomposition mechanisms of MHB are similar with MAB, where the hydrogen formation is due to the interaction between the $H^{\delta-}$ of the triangular structure (M···H···M) and the H^+ of the oligomer $[NH_2NHBH_2NH_2NHBH_3]^-$ unit [97,110]. The stability of MHB is dominated by the electronegativity of the metal. The MHB with high reactivity generally contains the center metal with low electronegativity. We summarized the properties of MHB in Table 6.

4. Amine metal borohydrides (AMB)

Except the MAB and MHB compounds summarized above, a large amount of amine metal borohydrides (AMB) are synthesized and studied in last ten years as one of the most promising candidates of hydrogen carriers. AMB is synthesized on the basis of mono or multi metal borohydrides ($M(BH_4)_n$ or $MM'(BH_4)_n$, M/M′ = Li/Na/Mg/Al/Ca/Zn/Sc/Ti/Zr/Y/Mn, etc) with NH_3 ligand [111–113]. The soft-donating ligands given by NH_3 to center metals stabilize $M(BH_4)_n$ compounds to form AMB, which exhibits extracting dehydrogenation performance and even potential reversibility. The typical AMB including the mono metal amine borohydrides and multi metal amine borohydrides with the corresponding derivatives are discussed in 4.1–4.8. The reported syngonies, crystal parameters and the dehydrogenation properties are summarized in Table 7. The typical bond lengths of AMBs are summarized in Table 8. The details of crystal structures of AMBs are listed in Fig. 4 and Fig. 5.

4.1. Ammine lithium borohydride (ALB) and its derivatives

4.1.1. Synthesis

$LiBH_4 \cdot xNH_3$ ($x = 1, 2, 3$) is synthesized by exposing $LiBH_4$ to NH_3 atmosphere at room temperature. Purified ammonia with 1.0 bar pressure reacts with $LiBH_4$ in a Schlenk tube for 20 min. Then the solid $LiBH_4 \cdot NH_3$ can be obtained by evacuating the tube for 3 h. The liquid $LiBH_4 \cdot 2NH_3$ can be obtained by reacting 1.0 bar ammonia with $LiBH_4$ in the tube for 30 min without pumping or shaking. The solid $LiBH_4 \cdot 3NH_3$ is synthesized by shaking and spreading liquid $LiBH_4 \cdot 2NH_3$ [132].

There are some derivatives designed for improving the dehydrogenation properties of $LiBH_4 \cdot NH_3$, such as Co-doped $LiBH_4 \cdot nNH_3$ (n = 1, 4/3, 2). A mixture of $CoCl_2$-$LiBH_4$ (with the molar ratio of 0.026:1) was mechanically milled at 200 rpm for 8 h to prepare Co-doped $LiBH_4$, which is further heated with ammonia in a small closed vessel to obtain homogeneous $LiBH_4 \cdot nNH_3$ (n = 1, 4/3, 2) [133].

$MgCl_2$-$LiBH_4 \cdot NH_3$, $ZnCl_2$-$LiBH_4 \cdot NH_3$, $AlCl_3$-$LiBH_4 \cdot NH_3$ composites were prepared by mixing $LiBH_4 \cdot NH_3$ with the corresponding additives. After hand milling for 5 min, the mixtures were heated to 65 °C for 5 min in a sealed bottle then cooled down to get the composites as shown in equation (16) [132].

$$MCl_n + LiBH_4 \cdot NH_3 \rightarrow LiCl + MCl_x(BH_4)_{n-x}(NH_3)_y + LiBH_4 \ (M = Mg/Zn/Al) \quad (16)$$

Similarly, $3LiH\text{-}3NH_3BH_3$-$LiBH_4 \cdot NH_3$ is prepared by grinding LiH-AB and $LiBH_4 \cdot NH_3$ for 10 min at a mole ratio of 3:1 handled in an argon-filled glove box [134]. This compound also showed improved dehydrogenation performance compared with that of ALBs.

4.1.2. Decomposition

$LiBH_4 \cdot NH_3$ mainly releases ammonia rather than hydrogen during the heating process. It starts to release ammonia at 40 °C and about 40 wt% ammonia is liberated before 160 °C [114]. H Hydrogen is gradually liberated after increasing the temperature above 280 °C [132]. $LiBH_4 \cdot NH_3$ can release 1.5 equiv. hydrogen in ammonia atmosphere below 300 °C [132]. With the dopant of $CoCl_2$, $LiBH_4 \cdot nNH_3$ (n = 1, 4/3, 2) releases 15.3 wt% (H-purity: 99.99%), 17.8 wt%, 14.3 wt% (H-purity: 97.60%) hydrogen at 250 °C, respectively. The products of the decomposed $LiBH_4 \cdot NH_3$ are LiH and BN. As for $LiBH_4 \cdot 2NH_3$, the final products are $LiNH_2$ and BN [133].

All the three $MgCl_2$-$LiBH_4 \cdot NH_3$, $ZnCl_2$-$LiBH_4 \cdot NH_3$ and $AlCl_3$-$LiBH_4 \cdot NH_3$ are heated in argon atmosphere. $ZnCl_2$-$LiBH_4 \cdot NH_3$ and $AlCl_3$-$LiBH_4 \cdot NH_3$ start to release hydrogen at 100–120 °C. $MgCl_2$-$LiBH_4 \cdot NH_3$ starts to release hydrogen around 170 °C. About 3.00, 2.49 and 2.94 equiv. hydrogen are liberated in the decomposition of $MgCl_2$-$LiBH_4 \cdot NH_3$, $AlCl_3$-$LiBH_4 \cdot NH_3$ and $ZnCl_2$-$LiBH_4 \cdot NH_3$, with ammonia contamination of 0.5 wt%, 1.3 wt% and 2.0 wt%, respectively [132].

As for $3LiH\text{-}3NH_3BH_3/LiBH_4 \cdot NH_3$, it releases *ca.* 10 wt% high-pure hydrogen (>99.9 mol%) below 100 °C with fast kinetics. The hydrogen emission of x $(LiH\text{-}NH_3BH_3)/LiBH_4 \cdot NH_3$ is from the combination of $H^{\delta+}$ (from $LiH\text{-}NH_3BH_3$) and $H^{\delta-}$ (from $LiBH_4 \cdot NH_3$), in which the controllable protic hydrogen source from the stabilized NH_3 group played a crucial role in providing optimal stoichiometric ratio of $H^{\delta+}$ and $H^{\delta-}$, and thus leading to the significant improvement of hydrogen capacity and purity [134].

4.1.3. Theoretical analysis

The band gap of solid $LiBH_4 \cdot NH_3$ is 5.72 eV. The coordinate bond N: → Li^+ in $LiBH_4 \cdot NH_3$ is easy to split to release ammonia at low temperature. The other dihydrogen bond of N-H···H-B is supposed to dominate the hydrogen release [132]. The ammonia removal energy of $LiBH_4 \cdot NH_3$ is 17.8 kcal/mol at room temperature based on DFT calculation [84]. $LiBH_4 \cdot NH_3$ releases hydrogen at high

Table 6
The dehydrogenation properties of MHB.

Compounds	Radius of center cations (Å)	Electroegativity of center cations	H content (Theor wt%)	H content (Exp wt% with the Temp)	Byproducts
HB [101]	–	–	15.28	12.2	Hydrazine
LiHB [102]	0.76	14.59	11.59	10.2 (400 °C)	N_2 &NH_3
LiHB·2HB [102]	0.76	14.59	13.54	11.5 (400 °C)	N_2
NaHB [103]	1.02	9.44	8.85	7.6 (150 °C)	NH_3 (slightly)
KHB [104]	1.38	6.47	7.16	7.3 (180 °C)	NH_3 (slightly)

Table 7
The syngony, groups, crystal parameters and the dehydrogenation properties of AMB.

Compound	Crystal structure	Properties of decompostion	
		H content (wt %)	Initial T_{dec} (°C)
$LiBH_4 \cdot NH_3$ [114]	*orthorhombic* system; *Pmmm* group; a = 5.968 Å, b = 4.463 Å, c = 14.342 Å.	4.0 (exp) 15.5 (Calc.)	40
$Mg(BH_4)_2 \cdot 6NH_3$ [115]	*Face-centereed cubic*; a = 10.82 Å	–	90 [116]
$Mg(BH_4)_2 \cdot 3NH_3$ [116]	*orthorhombic* system; a = 7.432 Å, b = 6.149 Å, c = 23.124 Å	24.83 (purity = 90.8%)	126
$Mg(BH_4)_2 \cdot 2NH_3$ [115]	*orthorhombic* system; *Pcab* group; a = 17.487 Å, b = 9.413 Å, c = 8.730 Å	15.9	120 [116]
$Mg(BH_4)_2 \cdot NH_3$ [116]	*orthorhombic* system; a = 11.335 Å, b = 7.690 Å, c = 6.927 Å	14.58 (purity = 99.8%)	138
$Ca(BH_4)_2 \cdot 4NH_3$ [117]	*monoclinic* system; $P2_1/c$ group; a = 6.448 Å, b = 12.104 Å, c = 7.242 Å	14.62	–
$Ca(BH_4)_2 \cdot 2NH_3$ [117]	*orthorhombic* system; *Pbcn* group; a = 6.416 Å, b = 8.390 Å, c = 12.702 Å	11.3	–
$Ca(BH_4)_2 \cdot NH_3$ [117,118]	*orthorhombic* system; $Pna2_1$ group; a = 8.202 Å, b = 11.857 Å, c = 5.838 Å	12.77	–
$Y(BH_4)_3 \cdot 7NH_3$ [119]	*orthorhombic* system; $Pca2_1$ group; a = 14.9569 Å, b = 8.4111 Å, c = 13.8122 Å	13.17	78
$Y(BH_4)_3 \cdot 6NH_3$ [119]	*Cubic* structure; *Pa-3* group; a = 12.339 Å	12.83	–
$Y(BH_4)_3 \cdot 5NH_3$ [119]	*Hexagonal* structure; *P63* group; a = 8.5476 Å, c = 9.941 Å	12.45	–
$Y(BH_4)_3 \cdot 4NH_3$ [119]	*orthorhombic* system; $Pna2_1$ group; a = 12.3869 Å, b = 7.1414 Å, c = 11.5313 Å	12.00	–
$Y(BH_4)_3 \cdot 4NH_3$ [120]	*orthorhombic* system; *Pc21n* group; a = 7.115 Å, b = 11.419 Å, c = 12.271 Å	8.7	60
$Y(BH_4)_3 \cdot 2NH_3$ [119]	*orthorhombic* system; *Pbca* group; a = 7.6126 Å, b = 12.0774 Å, c = 19,4662 Å	10.83	–
$Y(BH_4)_3 \cdot NH_3$ [119]	*orthorhombic* system; $Cmc2_1$ group; a = 7.8755 Å, b = 7.7449 Å, c = 12.2466 Å	10.05	–
$Ti(BH_4)_3 \cdot 3NH_3$ [121]	-	14	60
$Ti(BH_4)_3 \cdot 5NH_3$ [121]	-	13.4	75
$Mn(BH_4)_2 \cdot 6NH_3$ [122]	*Cubic* structure; *Fm3m* group; a = 10.8341 Å	14.0	–
$Mn(BH_4)_2 \cdot 3NH_3$ [122]	*orthorhombic* system; *Pnma* group; a = 11.4328 Å, b = 8.0869 Å, c = 9.4379 Å	12.6	–
$Mn(BH_4)_2 \cdot 3NH_3$ [122]	*orthorhombic* system; *Pcab* group; a = 17.484 Å, b = 9.4554 Å, c = 8.8731 Å	11.9	–
$V(BH_4)_3 \cdot 3NH_3$ [123]	*Cubic* structure; *F23* group; a = 10.7806 Å	14.3	65
$Fe(BH_4)_2 \cdot 6NH_3$ [124]	*Cubic* structure; *Fm3m* group; a = 10.7142 Å	14.0	63
$Co(BH_4)_2 \cdot 6NH_3$ [124]	*Cubic* structure; *Fm3m* group; a = 10.6724 Å	13.7	60
$Zn(BH_4)_2 \cdot 2NH_3$ [125]	*monoclinic* system; *P21* group; a = 6.392 Å, b = 8.417 Å, c = 6.388 Å, β = 92.407°	8.9	90
$Sr(BH_4)_2 \cdot NH_3$ [126]	*orthorhombic* system; *Pbcn* group; a = 6.816 Å, b = 8.619 Å, c = 20.776 Å	8.3	–
$Sr(BH_4)_2 \cdot 2NH_3$ [126]	*orthorhombic* system; *Pnc2* group; a = 6.5378 Å, b = 6.5455 Å, c = 8.5403 Å	9.3	70
$Sr(BH_4)_2 \cdot 4NH_3$ [126]	*monoclinic* system; *P21*/cgroup; a = 6.499 Å, b = 12.42 Å, c = 7.375 Å, β = 114.67°	10.9	–
$Zr(BH_4)_4 \cdot 8NH_3$ [127]	*orthorhombic* system; *Pbca* group; a = 16.76181 Å, b = 14.26414 Å, c = 13.65708 Å	22.8 (with NH_3)	60
$Gd(BH_4)_3 \cdot 7NH_3$ [119]	*orthorhombic* system; $Pca2_1$ group; a = 14.926 Å, b = 8.436 Å, c = 13.819 Å	10.36	82
$Gd(BH_4)_3 \cdot 6NH_3$ [119]	*cubic* system; *Pa-3* group; a = 12.3153 Å	9.95	–
$Gd(BH_4)_3 \cdot 5NH_3$ [119]	*Hexagonal* system; *P63* group; a = 8.6106 Å, c = 9.987 Å	9.48	–
$Gd(BH_4)_3 \cdot 4NH_3$ [119]	*orthorhombic* system; *Pc21n* group; a = 12.4458 Å, b = 7.2063 Å, c = 11.5819 Å	8.96	–
$Dy(BH_4)_3 \cdot 7NH_3$ [119]	*orthorhombic* system; $Pca2_1$ group; a = 14.83 Å, b = 8.433 Å, c = 13.74 Å	10.196	62
$Dy(BH_4)_3 \cdot 6NH_3$ [119]	*cubic* system; *Pa-3* group; a = 12.347 Å	9.78	–
$Dy(BH_4)_3 \cdot 5NH_3$ [119]	*Hexagonal* system; *P63* group; a = 8.629 Å, c = 9.891 Å	9.314	–
$Dy(BH_4)_3 \cdot 4NH_3$ [119]	*orthorhombic* system; *Pc21n* group; a = 12.337 Å, b = 7.185 Å, c = 11.508 Å	8.792	–
$LiMg(BH_4)_3 \cdot 2NH_3$ [128]	*Hexagonal* structure; *P63* group; a = 8.0002 Å, c = 8.4276 Å, γ = 120°	8 (exp)	<100
$Li_2Mg(BH_4)_4 \cdot 6NH_3$ [129]	*tetragonal* system; $P4_32_12$ group;	11.1	80

(*continued on next page*)

Table 7 (*continued*)

Compound	Crystal structure	Properties of decompostion	
		H content (wt %)	Initial T_{dec} (°C)
$Li_2Al(BH_4)_5·6NH_3$ [130]	a = 10.7656 Å, b = 13.843 Å, *hexagonal* system; *P*3*c*1 group; a = 7.798 Å, c = 15.969 Å	>10.0	~75
$LiSc(BH_4)_4·4NH_3$ [123]	*orthorhombic* system; *Pc21n* group; a = 7.438 Å, b = 11.154 Å, c = 14.513 Å	15.1	80
$Li_2Ti(BH_4)_3·5NH_3$ [121]	*orthorhombic* system; a = 18.283 Å, b = 10.216 Å, c = 7.954 Å	15.8	75
$Li_2Mn(BH_4)_4·6NH_3$ [122]	*Tetragonal* system; $P4_2/mnm$ group; a = 10.8177 Å, c = 6.9413 Å	14.9	–
$Li_2Fe(NH_3)_6(BH_4)_4$ [124]	*Tetragonal* system; $P4_2/mnm$ group; a = 10.7117 Å, c = 6.8963 Å	13.7	<80
$VMg(BH_4)_5·5NH_3$ [131]	*Monoclinic* system; *P*2/*m* group; a = 19.611 Å, b = 14.468 Å, c = 6.261 Å, β = 93.768°	12.4	65

Table 8
The reported bond length (Å) of typical AMB.

AMBs	M-N/M-B	$H^{\delta+}\cdots^{\delta-}H$	AMBs	M-N/M-B	$H^{\delta+}\cdots^{\delta-}H$
$LiBH_4·NH_3$ [114]	2.01/2.52–2.57	–	$Mn(BH_4)_2·3NH_3$ [122]	2.215,2.388/ 2.337,2.497	–
$Mg(BH_4)_2·2NH_3$ [115]	2.149,2.03/ 2.328,2.454	2.14	$V(BH_4)_3·3NH_3$ [123]	2.07/2.07	–
$Ca(BH_4)_2·2NH_3$ [117,125]	2.517/ 2.796,2.960	2.009	$Zn(BH_4)_2·2NH_3$ [101]	2.078/ 2.281,2.286	1.905
$Ca(BH_4)_2·NH_3$ [117,118]	2.50	–	$Sr(BH_4)_2·NH_3$ [126]	2.69/2.86–3.16	2.035
$Y(BH_4)_3·7NH_3$ [119]	2.47–2.51/ 4.30–4.97	1.85	$Sr(BH_4)_2·2NH_3$ [126]	2.71/2.85,3.10	1.92
$Y(BH_4)_3·6NH_3$ [119]	2.47–2.48/ 5.04–5.45	1.854	$Sr(BH_4)_2·4NH_3$ [126]	2.69–2.70/2.93	2.009
$Y(BH_4)_3·5NH_3$ [119]	2.40–2.58/3.13	2.209	$Zr(BH_4)_4·8NH_3$ [127]	2.15–2.67	–
$Y(BH_4)_3·4NH_3$ [119]	2.44–2.49/2.80–2.83	1.864	$LiMg(BH_4)_3·2NH_3$ [128]	Li-B:2.31–2.51 Mg-N:2.04–2.20	2.19–2.27
$Y(BH_4)_3·4NH_3$ [120]	2.416–3.036/ 2.419–2.431	1.951	$Li_2Mg(BH_4)_4·6NH_3$ [129]	Li-B:2.455–2.587 Mg-N:2.128–2.298	1.868
$Y(BH_4)_3·2NH_3$ [119]	2.51/2.53–2.80	2.033	$Li_2Al(BH_4)_5·6NH_3$ [130]	Li-B:2.52–2.58 Al-N:1.62–2.01	2.02–2.26
$Y(BH_4)_3·NH_3$ [119]	2.48/2.50–2.80	2.014	$LiSc(BH_4)_4·4NH_3$ [123]	Sc-N:2.32–2.44 Sc-B:2.27–2.59	1.92
$Mn(BH_4)_2·6NH_3$ [122]	2.267	–	$Li_2Mn(BH_4)_4·6NH_3$ [122]	Li-B:2.534–2.696 Mn-N:2.515–2.674	–
$Mn(BH_4)_2·3NH_3$ [122]	2.163,2.205/ 2.518,2.497	2.189			

temperature because of the formation of LiAB structure. A large amount of hydrogen is generated by the combination of the H radicals [135].

4.2. Divalence metal ammine borohydrides and their derivatives (metal = Mg/Ca/Sr/Mn/Fe/Co/Zn)

4.2.1. Ammine borohydrides with magnesium

4.2.1.1. Synthesis. $Mg(BH_4)_2·6NH_3$ was first prepared by electrolysis of alkali-metal borohydrides with Mg anode in liquid ammonia [136] where the pure $Mg(BH_4)_2·6NH_3$ is obtained by the reaction of liquid ammonia and $Mg(BH_4)_2$ etherate in ether at low temperature [136,137]. The further decomposition of $Mg(BH_4)_2·6NH_3$ in a vacuum at 125 °C generates $Mg(BH_4)_2·2NH_3$ [136]. Actually, $Mg(BH_4)_2·nNH_3$ (n = 1–5) can be prepared by directly ball milling the mixtures of $Mg(BH_4)_2·6NH_3$ and $Mg(BH_4)_2$ as showed in equation (17) [116].

$$nMg(BH_4)_2·6NH_3 + (6\text{-}n)\,Mg(BH_4)_2 \rightarrow 6\,Mg(BH_4)_2·nNH_3 \quad (17)$$

$Mg(BH_4)_2·6NH_3$ nanoparticles also appear excellent dehydrogenation properties, which are synthesized by filling NH_3 gas into the diethyl ether solution of $Mg(BH_4)_2·2Et_2O$ under ultrasound conditions. The white powdery solid $Mg(BH_4)_2·6NH_3$ with particle size in the range of 20–40 nm [138].

The F-substituted $Mg(BH_4)_2·2NH_3$ is successfully prepared by a mechano chemical reaction of $Mg(BH_4)_2·2NH_3$ and $LiBF_4$, which shows very attractive dehydrogenation properties [139].

There are two methods by doping other hydrogen storage materials to improve the dehydrogenation properties of $Mg(BH_4)_2·nNH_3$. Pan et al. found $NaAlH_4$ is an excellent dopant of $Mg(BH_4)_2·nNH_3$ for enhancing its dehydrogenation properties, where the $Mg(BH_4)_2·2NH_3$-x$NaAlH_4$ (x = 1–4) composites are prepared by ball milling (200 rpm for 1 h) $Mg(BH_4)_2·2NH_3$ and $NaAlH_4$ with different molar ratios [140].

Except for $Mg(BH_4)_2·2NH_3$ - x$NaAlH_4$, NH_3BH_3 is an outstanding candidate of the dopant. The $Mg(BH_4)_2·6NH_3$-nNH_3BH_3-$ZnCl_2$ is synthesized by Yu et al. $Mg(BH_4)_2·2NH_3$/AB with molar ratios of 1:1, 1:2, 1:5 and 1:6 are first prepared by ball milling at 260 rpm for 4 h. Furthermore, the mixtures of $Mg(BH_4)_2·6NH_3$-nNH_3BH_3 and $ZnCl_2$ with the molar ratio of 2:1, 4:1 and 8:1 are mechanically milled at 260 rpm for 4 h in argon, resulting the formation of the $ZnCl_2$ doped $Mg(BH_4)_2·6NH_3$-nNH_3BH_3 system [141].

4.2.1.2. Decomposition. The onset decomposition temperature of $Mg(BH_4)_2·nNH_3$ (n = 1, 2, 3, and 6) is 138 °C/120 °C/126 °C/90 °C,

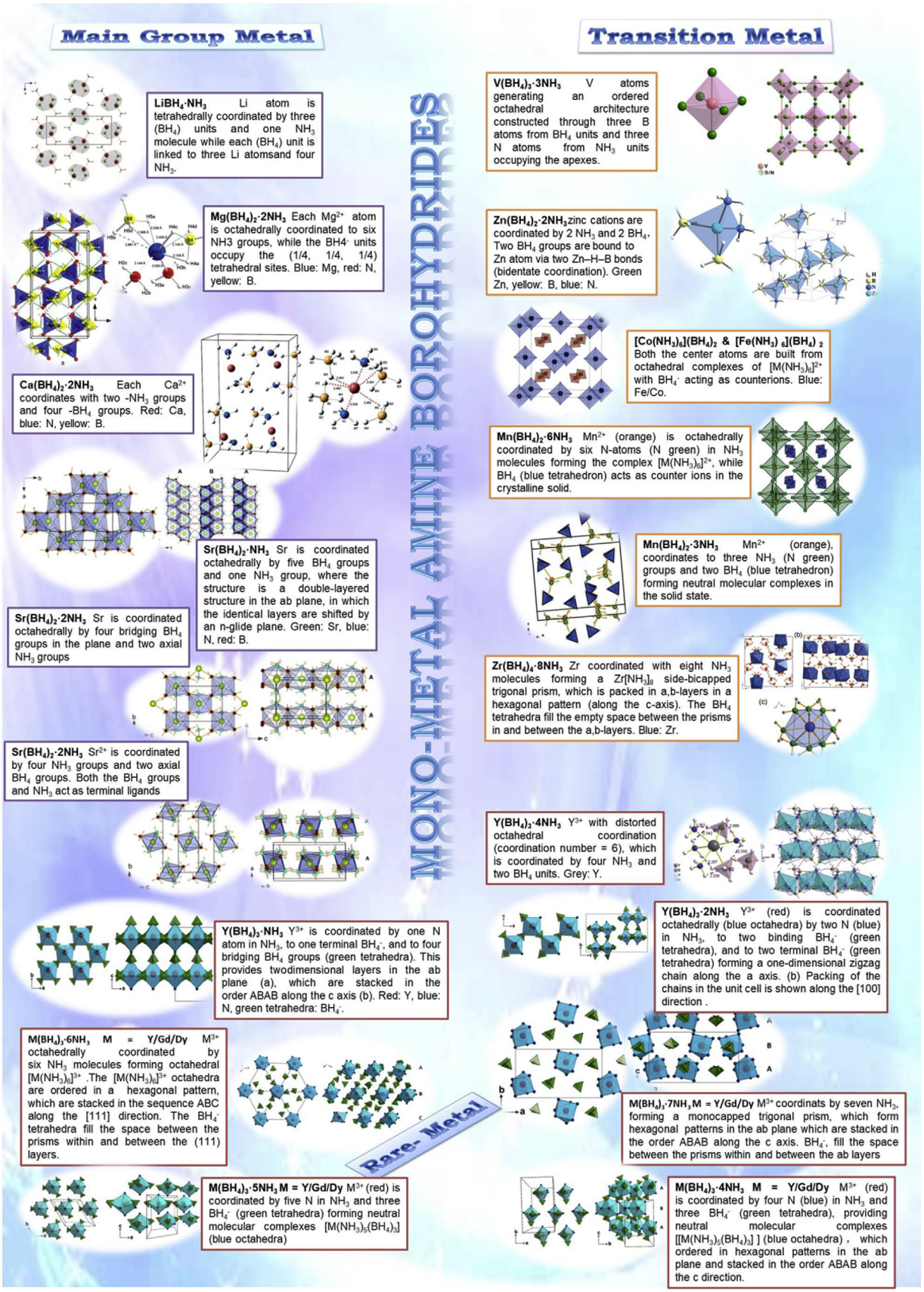

Fig. 4. Crystal structures of Mono-metal amine borohydrides.

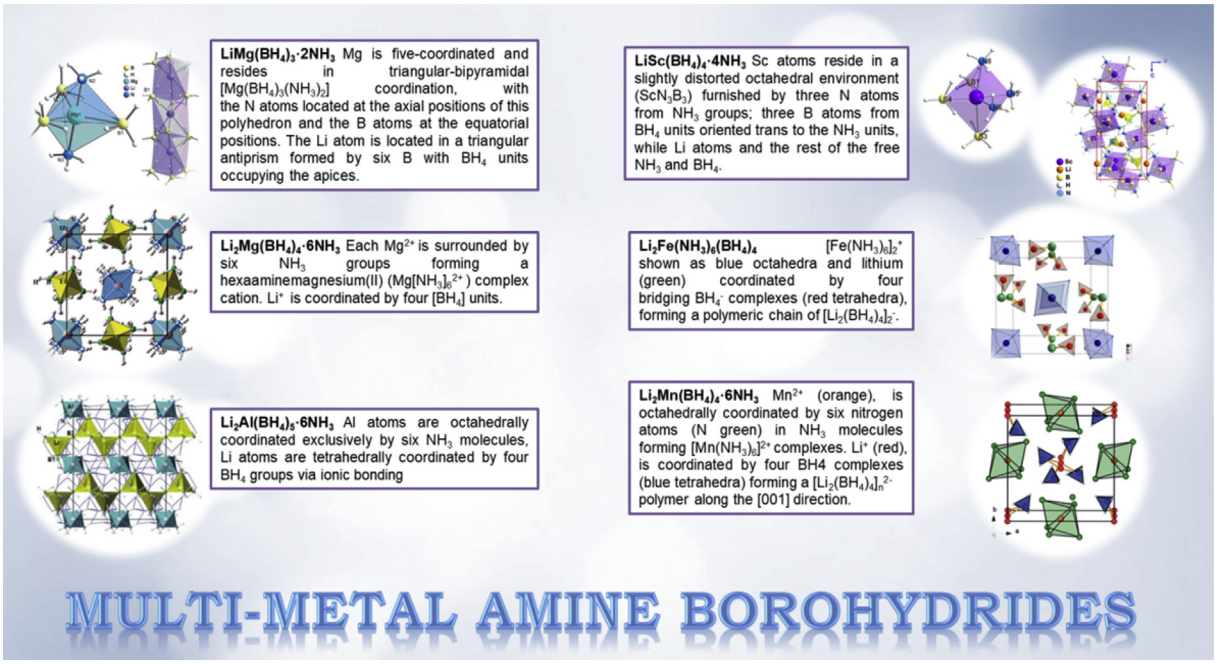

Fig. 5. Crystal structures of Multi-metal amine borohydrides.

respectively. As a consequence, the purities of H_2 were calculated to be 99.8, 97.1, 90.8, and 63.7 mol% for n = 1, 2, 3, and 6 of $Mg(BH_4)_2 \cdot nNH_3$, respectively [116].

The heating of $Mg(BH_4)_2 \cdot 6NH_3$ at 118 °C in a vacuum for 4 h produced about 4 equiv. of ammonia and the diammoniate complex $Mg(BH_4)_2 \cdot 2NH_3$ [115]. The results show that the quantities of hydrogen release of $Mg(BH_4)_2 \cdot 6NH_3$ is 13.3 wt% with the purity of 59% [115,138]. $Mg(BH_4)_2 \cdot 2NH_3$ releases 15.9 wt% hydrogen until 500 °C. Additionally, $Mg(BH_4)_2 \cdot 6NH_3$ nanoparticles start to release hydrogen below 30 °C and a total of 14.5 wt% hydrogen is released at 30–450 °C with the hydrogen purity of 71% [138].

Hydrogen release from the F-substituted $Mg(BH_4)_2 \cdot 2NH_3$ is started at approximately 70 °C. At 150 °C, the 15 mol% F-substituted sample could release 5.2 wt% of hydrogen within 40 min [139].

The dehydrogenation process of $Mg(BH_4)_2 \cdot 2NH_3$-$xNaAlH_4$ (x = 1–4) starts at 70 °C with approximately 11.3 wt% hydrogen released until 570 °C. The dehydrogenated products can take up ~3.5 wt % of hydrogen at 450 °C and 100 bar of hydrogen pressure, exhibiting a partial reversibility for hydrogen storage [140].

$Mg(BH_4)_2 \cdot 6NH_3$-nNH_3BH_3-$ZnCl_2$ (n = 0.5) composite is shown to release over 7 wt% high-pure hydrogen (>99 mol%) at 95 °C within 10 min, in which the $ZnCl_2$ plays a crucial role in stabilizing the NH_3 groups and promoting the recombination of $NH^{\delta+} \cdots {}^{-\delta}HB$ [141].

4.2.1.3. Theoretical analysis. The band gap of $Mg(BH_4)_2 \cdot 2NH_3$ is 6.0 eV (578.34 kJ/mol), where Mg^{2+} appears very high ionic character and plays as the electron donor in the compound based on the DFT calculation [142]. Hydrogen is released through the combination of large amount H ions, which is caused by the intensive vibrations of B-H and N-H bonds with increased temperature based on the CPMD simulation [135]. Caused by the strong polarization of Mg^{2+}, it bonds with N and B very stable, which appears excellent dehydrogenation performance. The formation of hydrogen is easy to generate on the surface with the formation energy of 0.79 eV (76.15 kJ/mol), which is considerably lower than that of the formation of ammonia. As for $Mg(BH_4)_2 \cdot 6NH_3$ nanoparticles, the theoretical investigation indicated that BN and $Mg_3B_xN_{x+2}$ compound were formed with the generation of 8 mol H_2 and 10/3 mol NH_3 during the decomposition [138].

For F-substituted $Mg(BH_4)_2 \cdot 2NH_3$, F-substitution induces more ionized $H^{\delta-}$ in the ammoniate and facilitates the local $H^{\delta+}$-$H^{\delta-}$ combinations in the $Mg(BH_4)_2 \cdot 2NH_3$ molecule. F substitution weakens the Mg-B bonds in $Mg(BH_4)_2 \cdot 2NH_3$ but favours the generation of B–N bonds during dehydrogenation [139].

4.2.2. Ammine borohydrides with calcium and strontium

4.2.2.1. Synthesis. $Ca(BH_4)_2 \cdot 6NH_3$ can be obtained by introducing anhydrous ammonia into $Ca(BH_4)_2$ at room temperature. The relationship among the four kinds of $Ca(BH_4)_2 \cdot xNH_3$ (x = 1, 2, 4, 6) are showed as in Scheme 1 [117].

In order to improve the properties in its dehydrogenation, The mixture of $Ca(BH_4)_2 \cdot NH_3$-$LiBH_4$ with the mole ratio of 1:1 is mechanically milled for 60 min under argon atmosphere. The synthesis and possible decomposition is summarized as equation (19) [118].

$$\begin{array}{l} Ca(BH_4)_2(NH_3) + LiBH_4 \xrightarrow{Syn} LiCa(NB_3H_9) + 3H_2 \\ \qquad\qquad\qquad\qquad\qquad\qquad\quad \downarrow Dec \\ [Li_4B_{10}H_6] + Ca_3B_2N_4 + CaH_2 + 14H_2 \end{array} \tag{19}$$

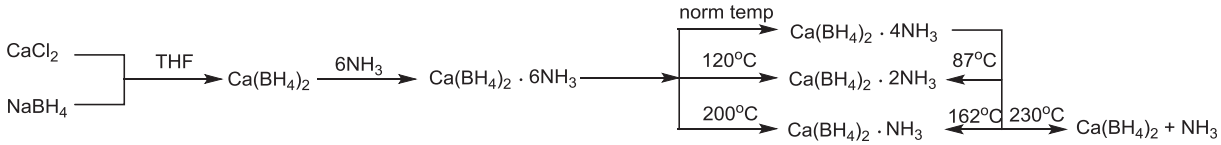

Scheme 1. The relationship among the four kinds of $Ca(BH_4)_2{\cdot}xNH_3$ (x = 1, 2, 4, 6).

$Mg(BH_4)_2$ can be used as a dopant to improve the performances of $Ca(BH_4)_2{\cdot}xNH_3$ in the decomposition. The mixtures of $Ca(BH_4)_2{\cdot}4NH_3$ and $Mg(BH_4)_2$ with mole ratios of 1:1 and 1:2 are mixed and ball milled for 4 h in an argon filled glove box. Similarly, the other $Mg(BH_4)_2$ doped $Ca(BH_4)_2{\cdot}xNH_3$ are obtained by ball milling $Ca(BH_4)_2{\cdot}2NH_3/Mg(BH_4)_2$ with the mole ratio of 1:1, or $Ca(BH_4)_2{\cdot}NH_3/Mg(BH_4)_2$ with the mole ratio of 1:1, respectively [143].

$Sr(BH_4)_2{\cdot}4NH_3$ is directly obtained by passing anhydrous ammonia (<33 ppm) over $Sr(BH_4)_2$ for 1–2 h at −5 °C, which is an unstable structure at room temperature. $Sr(BH_4)_2{\cdot}4NH_3$ decomposes to form $Sr(BH_4)_2{\cdot}2NH_3$ when putting it in the vacuum environment for 10 min. $Sr(BH_4)_2{\cdot}NH_3$ is prepared by treating the mixture of $Sr(BH_4)_2{\cdot}2NH_3$ and $Sr(BH_4)_2$ with the mole ratio of 1:1 mechanochemically [126].

4.2.2.2. Decomposition. Decomposition of $Ca(BH_4)_2{\cdot}6NH_3$ under a vacuum at room temperature for 20 min gives the formation of $Ca(BH_4)_2{\cdot}4NH_3$.

The decomposition of $Ca(BH_4)_2{\cdot}4NH_3$ from RT to 200 °C includes 3 distinct mass losses, 1) 2 equiv. NH_3 liberation (20 wt%) at RT ~ 85 °C, 2) the generation of $Ca(BH_4)_2{\cdot}2NH_3$ at 100–140 °C after a second liberation of ammonia (9.3 wt%), 3) further deammoniation (8.6 wt%) between 150 and 200 °C to produce $Ca(BH_4)_2$ [126].

The decomposition of $Ca(BH_4)_2{\cdot}2NH_3$ under the dynamic flow mode (TPD or TG-DSC) evolves 2 equiv of ammonia and little hydrogen below 300 °C. However, when conducting volumetric release measurement in a closed vessel, the low equilibrium pressure of NH_3 is showed in the $Ca(BH_4)_2{\cdot}2NH_3$ system below 180 °C. A rapid pressure increase can be observed when the temperature was above 200 °C. Hydrogen of *ca.* 5.9 equiv. (or 11.3 wt%) is released from $Ca(BH_4)_2{\cdot}2NH_3$ upon heating the sample to 500 °C [117].

$Ca(BH_4)_2{\cdot}NH_3$-$LiBH_4$ releases hydrogen from 80 °C and appears tremendous suppression of ammonia formation in the decomposition. Only the hydrogen liberation is observed in the mixture in the decomposition with the total weight loss of 12.3 wt% by 350 °C [118].

The $Mg(BH_4)_2$ doped $Ca(BH_4)_2{\cdot}nNH_3$ is studied by Yu's group. $Ca(BH_4)_2{\cdot}4NH_3$-$Mg(BH_4)_2$ (1:1) starts to dehydrogenation at ~62 °C and releases more than 9 wt % hydrogen below 300 °C with the purity of 92.3 wt %. $Ca(BH_4)_2{\cdot}4NH_3$-$Mg(BH_4)_2$ (1:2), $Ca(BH_4)_2{\cdot}2NH_3$-$Mg(BH_4)_2$ (1:1) and $Ca(BH_4)_2{\cdot}NH_3$-$Mg(BH_4)_2$ (1:1) evolve 7.2, 8.6 and 6.4 wt% hydrogen (with all the purities of hydrogen > 99%), respectively [143].

The TGA data for $Sr(BH_4)_2{\cdot}2NH_3$ reveals a two-step decomposition with a total mass loss of 16 wt % at 80–160 °C, which corresponds to the liberation of two equiv. NH_3 (theoretically 22.6 wt %). The maximum liberation of NH_3 appears at 133 and 160 °C confirmed by MS analysis. Upon further heat treatment, a mass loss of 2 wt % is revealed from 385 to 435 °C at the same time as an endothermic event with minima at 392 °C caused by the thermal decomposition of $Sr(BH_4)_2$ [126].

4.2.3. Ammine borohydrides with manganese

4.2.3.1. Synthesis. $Mn(BH_4)_2$ is first synthesized by the metathesis reaction between $MnCl_2$ and $LiBH_4$ with the ratio of 1:2 in anhydrous diethyl ether for 12 h. Then $Mn(BH_4)_2$ reacts with anhydrous ammonia directly for 2–3 h to generate $Mn(BH_4)_2{\cdot}6NH_3$. The different $Mn(BH_4)_2{\cdot}xNH_3$ (x = 1, 2, 3, 6) compounds can be prepared based on $Mn(BH_4)_2{\cdot}6NH_3$ (as showed in Table 9) [122]. All the powders of the reactants in Table 9 are ball milled at 250 rpm for 2 min intervened by a 2 min break for repeating 60 times.

4.2.3.2. Decomposition. $Mn(BH_4)_2{\cdot}6NH_3$, $Mn(BH_4)_2{\cdot}3NH_3$ and $Mn(BH_4)_2{\cdot}NH_3$ all release minor amounts of ammonia at higher temperature. $Mn(BH_4)_2{\cdot}NH_3$ releases mainly hydrogen with traces of NH_3, where the peak of mass loss is around 130 °C. The decomposition temperatures of $Mn(BH_4)_2{\cdot}xNH_3$ (x = 1, 2, 3, 6) and the released gases with the $[NH_3]/[BH_4]$ ratios are summarized in Fig. 6 [122].

4.2.4. Ammine borohydrides with iron/cobalt/zinc

4.2.4.1. Synthesis. $Fe(BH_4)_2$ is first obtain ned by stirring $FeCl_2$ and $LiBH_4$ in $S(CH_3)_2$ solution for 4 h. Then $Fe(BH_4)_2{\cdot}6NH_3$ is prepared by the reaction between $Fe(BH_4)_2$ and NH_3 gas [124]. Similarly, $Co(BH_4)_2{\cdot}6NH_3$ is prepared by the reaction between $CoCl_2$ and $LiBH_4$ in liquid ammonia, where the productivity of the synthesis is 40 wt% [124].

$Zn(BH_4)_3{\cdot}2NH_3$ is prepared by ball milling $ZnCl_2{\cdot}2NH_3$ and $LiBH_4$ with the ratio of 1:2, where the pre-synthesis of $ZnCl_2{\cdot}2NH_3$ is accomplished by the reaction of MBH_4 (M = Li/K/Ca) and $ZnCl_2$ in Et_2O solution [125].

4.2.4.2. Decomposition. $Fe(BH_4)_2{\cdot}6NH_3$ releases a mixture of hydrogen and ammonia up to 35 wt% in a single step below 100 °C (with the peaks of mass loss at 74 °C for NH_3 and 78 °C for H_2). The unpurified mixture after synthesis containing (0.59 $Fe(BH_4)_2{\cdot}6NH_3$ + 0.16 $Fe(NH_3)_6Cl_2$ + 0.25 LiCl) wt% reveals a total mass loss of 35 wt% [124]. As for the decomposition of $Co(BH_4)_2{\cdot}6NH_3$, the mixture containing $Co(BH_4)_2{\cdot}6NH_3$ (0.40 $Co(BH_4)_2{\cdot}6NH_3$ + 0.21 $Co(NH_3)_6Cl_2$ + 0.16 $Co(NH_3)_6(BH_4)_{2-x}Cl_x$ + 0.08 LiCl + 0.15 $LiCl{\cdot}6NH_3$ (wt%)) reveals a total mass loss

Table 9
Different $Mn(BH_4)_2{\cdot}xNH_3$ (x = 1, 2, 3, 6) compounds generated from mechanochemical dispose (from Ref. [122]).

Reactants	Products
$Mn(BH_4)_2$+excess of NH_3 + remaining $LiBH_4$	$Mn(BH_4)_2{\cdot}6NH_3$ (95.4 wt%), $Li_2Mn(BH_4)_4{\cdot}6NH_3$ (4.6 wt%)
$Mn(BH_4)_2$ ($S(CH_3)_2$)+excess of NH_3 + remaining $LiBH_4$	$Mn(BH_4)_2{\cdot}6NH_3$ (~95 wt%), $Li_2Mn(BH_4)_4{\cdot}6NH_3$ (~5 wt%)
$Mn(BH_4)_2{\cdot}6NH_3$- $Mn(BH_4)_2$ (5:1) + remaining $LiBH_4$	$Mn(BH_4)_2{\cdot}6NH_3$ (47.0 wt%), $Mn(BH_4)_2{\cdot}3NH_3$ (31.5 wt%), $Li_2Mn(BH_4)_4{\cdot}6NH_3$ (21.5 wt%)
$Mn(BH_4)_2{\cdot}6NH_3$- $Mn(BH_4)_2$ (4:2) + remaining $LiBH_4$	$Mn(BH_4)_2{\cdot}3NH_3$ (50.2 wt%), $Mn(BH_4)_2{\cdot}6NH_3$ (29.9 wt%), $Li_2Mn(BH_4)_4{\cdot}6NH_3$ (18.9 wt%), $Mn(BH_4)_2{\cdot}2NH_3$ (1.1 wt%)
$Mn(BH_4)_2{\cdot}6NH_3$- $Mn(BH_4)_2$ (3:3) + remaining $LiBH_4$	$Mn(BH_4)_2{\cdot}3NH_3$ (75.7 wt%), $Li_2Mn(BH_4)_4{\cdot}6NH_3$ (20.7 wt%), $Mn(BH_4)_2{\cdot}6NH_3$ (2.4 wt%), $Mn(BH_4)_2{\cdot}2NH_3$ (1.3 wt%)
$Mn(BH_4)_2{\cdot}6NH_3$- $Mn(BH_4)_2$ (2:4) + remaining $LiBH_4$	$Mn(BH_4)_2{\cdot}2NH_3$ (~95 wt%), unidentified Compd (~5 wt%)

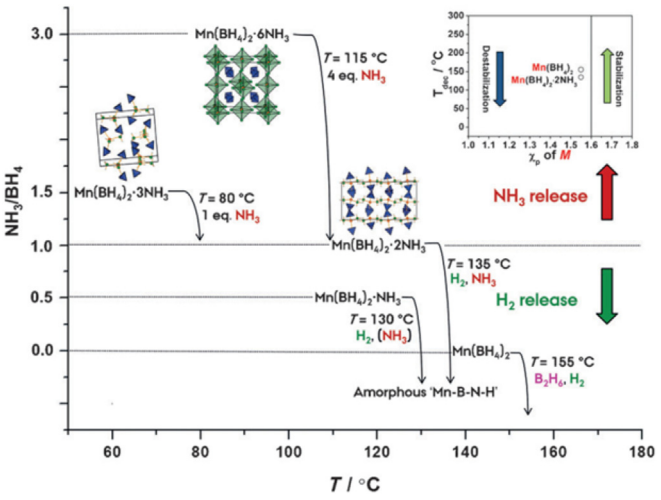

Fig. 6. The decomposition temperatures of $Mn(BH_4)_2 \cdot xNH_3$ (x = 1, 2, 3, 6) and released gases with the $[NH_3]/[BH_4]$ ratios from Ref. [122].

of 29 wt% [124].

$Zn(BH_4)_3 \cdot 2NH_3$ starts to release pure hydrogen at around 90 °C and ends before 150 °C with a peak at 127 °C. Totally 8.9 wt% hydrogen is released from $Zn(BH_4)_3 \cdot 2NH_3$ with high purity [125].

4.2.4.3. Theoretical analysis. The band gap of $Zn(BH_4)_3 \cdot 2NH_3$ is 5.5 eV (530.15 kJ/mol) by using GGA-PBE method with the cutoff energy of 650 eV. The initial dehydrogenation of $Zn(BH_4)_3 \cdot 2NH_3$ is achieved by the dissociation of $H(N)^{\delta+} \cdots {}^{\delta-}H(B)$, which results in the formation of N-B dative bond before the continuous dehydrogenation [142].

4.3. Tervalence metal ammine borohydrides and their derivatives ($M(BH_4)_3 \cdot nNH_3$ M = Al/Y/Ti/V)

4.3.1. Ammine borohydrides with aluminum

4.3.1.1. Synthesis. $Al(BH_4)_3 \cdot 6NH_3$ is prepared by passing a stream of $Al(BH_4)_3$, diluted in argon and purified by aluminum powder, into dry ammonia at around 0 °C for more than 6 h [144]. $Al(BH_4)_3 \cdot nNH_3$ (n = 5, 4, 3, 2) is obtained by the reaction between $Al(BH_4)_3 \cdot 6NH_3$ and $Al(BH_4)_3$. The derivatives such as the $Al(BH_4)_3 \cdot nNH_3$ - $xLiBH_4$ (n = 5, 4, 3; x = 1, 2) are prepared by ball-milling the mixtures of $Al(BH_4)_3 \cdot nNH_3$ and $LiBH_4$ [145].

4.3.1.2. Decomposition. The dehydrogenation of $Al(BH_4)_3 \cdot 6NH_3$ is in the temperature range of 60–180 °C with the contamination of ammonia. No B_2H_6 and polymerized NHBH are detected during the decomposition. A total of 11.8 wt% hydrogen is liberated with a purity of 94.6% after heating the sample to 300 °C. The details for the decomposition of these compounds can be found in Table 10 [146]. The capacity and purity of H_2 are determined below 350 °C. The impurities are suppressed in $Al(BH_4)_3 \cdot 4NH_3$ and $Al(BH_4)_3 \cdot 3NH_3$. $Al(BH_4)_3 \cdot 4NH_3$ - $LiBH_4$ as a derivative releases 12 wt% pure hydrogen at 120 °C [145].

The combination of $Al(BH_4)_3 \cdot 6NH_3$ and AB is also reported by Yu's groups for the generation of $Al(BH_4)_3 \cdot 6NH_3$-4AB and $Li_2Al(BH_4)_5(NH_3BH_3)_3 \cdot 6NH_3$, both of which release 11 wt% hydrogen with the purities of more than 98 mol% at below 120 °C [145].

4.3.2. Ammine borohydrides with yttrium/titanium/vanadium

4.3.2.1. Synthesis. In the synthesis process, $YCl_3 \cdot 4NH_3$ is first prepared after the formation of $YCl_3 \cdot 7NH_3$ by exposing YCl_3 to NH_3 atmosphere. Then the mixture of $YCl_3 \cdot 4NH_3$-$LiBH_4$ with the molar ratio of 1:3 is mechanically milled for 60 min under argon to obtain $Y(BH_4)_3 \cdot 4NH_3$ [120].

$TiCl_3 \cdot 5NH_3$ and $TiCl_3 \cdot 3NH_3$ are the precursors of $Ti(BH_4)_3 \cdot 5NH_3$ and $Ti(BH_4)_3 \cdot 3NH_3$, which can be first prepared by exposing $TiCl_3$ to NH_3 atmosphere, where $Ti(BH_4)_3 \cdot 3NH_3$ is obtained by keeping $Ti(BH_4)_3 \cdot 5NH_3$ and $TiCl_3$ together at 200 °C for at least 24 h $TiCl_3 \cdot 5NH_3$ and $LiBH_4$ (or the $TiCl_3 \cdot 3NH_3$ and $LiBH_4$) are ball-milled with the molar ratio of 1:3 to obtain $Ti(BH_4)_3 \cdot 5NH_3$ ($Ti(BH_4)_3 \cdot 3NH_3$) [121].

$VCl_3 \cdot 5NH_3$ was prepared by exposing VCl_5 powders to NH_3 atmosphere. $V(BH_4)_3 \cdot 5NH_3$ is synthesized via ball-milling $VCl_3 \cdot 5NH_3$ and $LiBH_4$ with the mole ratio of 1:3 [131]. Heat treatment of $VCl_3 \cdot 5NH_3$ at 250 °C is for the synthesis of $VCl_3 \cdot 3NH_3$ [123]. Then $V(BH_4)_3 \cdot 3NH_3$ is finally synthesized by ball-milling the mixture of $LiBH_4$ and $VCl_3 \cdot 3NH_3$ with the mole ratio of 3:1 [123].

4.3.2.2. Decomposition. $Y(BH_4)_3 \cdot 4NH_3$ starts to decompose at 60 °C with notable ammonia emission. There are three peaks of mass loss at 86 °C, 179 °C and 279 °C, respectively. Isothermal decomposition of $Y(BH_4)_3 \cdot 4NH_3$ at 200 °C revealed that over 8.7 wt% hydrogen can be released totally [120].

$Ti(BH_4)_3 \cdot 3NH_3$ starts to release hydrogen from 60 °C, and it releases 14 wt% pure H_2 until 300 °C including the three peaks of mass loss at 105, 120 and 215 °C, respectively. $Ti(BH_4)_3 \cdot 5NH_3$ starts to release hydrogen from 75 °C, and ~13.1 wt% H_2 accompanied with a small amount of ammonia is liberated upon heating the sample to 200 °C (the purity of hydrogen is 96%) [121].

The decomposition of $V(BH_4)_3 \cdot 5NH_3$ includes two temperature ranges of 80–110 °C and 110–250 °C, respectively. There is about 11.5 wt% hydrogen released from room temperature to 400 °C with a hydrogen purity of 85% [131]. There are two steps in the decomposition process of $V(BH_4)_3 \cdot 3NH_3$ by MS/TG measurement. The first one entails the pure hydrogen emission occurring in the temperature at 65–90 °C with the sharp peak at 79 °C. The second one from 90 to 190 °C is dominated by hydrogen liberation accompanied by a slight amount of ammonia release. A total of 16.1 wt% hydrogen of $V(BH_4)_3 \cdot 3NH_3$ with the hydrogen purity of 99% can be reached until 300 °C [123].

Table 10
Calculated capacity and purity of H_2 released from $Al(BH_4)_3 \cdot nNH_3$ and its composites (Ref [146]).

Sample	H_2 capacity (wt%)	H_2 purity (%)	Peak (°C)	Main purity
$Al(BH_4)_3 \cdot 6NH_3$	11.8	67.4	168	NH_3
$Al(BH_4)_3 \cdot 5NH_3$	16.8	90.6	159	NH_3
$Al(BH_4)_3 \cdot 4NH_3$	15.5	>99	128	–
$Al(BH_4)_3 \cdot 3NH_3$	13.7	>99	113	–
$Al(BH_4)_3 \cdot 2NH_3$	13.7	66.6	108	B_2H_6
$Al(BH_4)_3 \cdot 5NH_3$ - $LiBH_4$	15.4	81.0	145	NH_3
$Al(BH_4)_3 \cdot 5NH_3$ - $2LiBH_4$	15.8	92.4	142	NH_3
$Al(BH_4)_3 \cdot 4NH_3$ - $LiBH_4$	16.1	>99	109, 128	–
$Al(BH_4)_3 \cdot 4NH_3$ - $2LiBH_4$	14.2	96.6	121	B_2H_6

4.4. Ammine borohydrides with zirconium/niobium and lanthanide metals (gadolinium/dysprosium)

4.4.1. Synthesis

For Zirconium amine borohydrides, the solvent-free $Zr(BH_4)_4$ is first prepared by ball-milling $LiBH_4$ and $ZrCl_4$ powders in the solid phase, and then the produced $Zr(BH_4)_4$ is exposed to anhydrous ammonia in an ice-water bath to synthesize $Zr(BH_4)_4 \cdot 8NH_3$ [127].

$NbCl_5 \cdot 5NH_3$ was first fabricated by exposing $NbCl_5$ powder to NH_3 atmosphere. Then $NbCl_5 \cdot 5NH_3$-MBH_4 (M = Li, Na) with a mole ratio of 1:5 is mechanically milled for 120 min at 350 rpm under argon atmosphere [147].

$$M(BH_4)_3 \cdot 7NH_3 \rightarrow M(BH_4)_3 \cdot 6NH_3 + NH_3 \rightarrow M(BH_4)_3 \cdot 5NH_3 + NH_3 \rightarrow M(BH_4)_3 \cdot 4NH_3 + NH_3 \quad (20)$$

For both Lanthanide metal ammine borohydrides, $M(BH_4)_3 \cdot 7NH_3$ (M = Gd, Dy) are obtained by the reaction between $Gd(BH_4)_3$ (or $Dy(BH_4)_3$) and NH_3 with a ratio of 1:7 at room temperature. Other Lanthanide metal ammine borohydrides with less NH_3 ligands can be obtained via the decomposition of $M(BH_4)_3 \cdot 7NH_3$ as showed in equation (20) [119].

4.4.2. Decomposition

$Zr(BH_4)_4 \cdot 8NH_3$ starts to release hydrogen at 60 °C with the peak of mass loss at 130 °C accompanied by the release of a small amount of ammonia. A total weight loss of 22.8 wt% at 300 °C was attributed to the liberation of H_2 and NH_3. There are 4.8 wt%, 6.1 wt%, 7.6 wt% and 8.5 wt% of hydrogen released in this compound at 90 °C, 110 °C, 130 °C and 150 °C, respectively [127].

$NbCl_5 \cdot 5NH_3$-$5LiBH_4$ releases 8.1 wt% hydrogen from 50 to 250 °C by a two-step dehydrogenation process with peaks of mass loss at 98 and 165 °C, respectively. No ammonia and boranes are detected in the process. $NbCl_5 \cdot 5NH_3$-$5NaBH_4$ starts to release hydrogen at 65 °C. A total of 11.2 wt% pure hydrogen is released until 250 °C with two peaks at 95 and 140 °C, respectively. Dehydrogenation mechanism revealed that in addition to the combination of NH/HB between the NH_3 and BH_4 groups that facilitates the H_2 release, the BH/HB and NH/HN homo-polar interactions also contribute to the H_2 formation. The combination of NH/HN is due to the effect of Nb^{5+} working as an accelerant to promote the NH_3 crack [147].

The mass loss of $Gd(BH_4)_3 \cdot 7NH_3$ is 19.5 wt% at 125 °C with the hydrogen and ammonia liberation. TGA data for $Dy(BH_4)_3 \cdot 7NH_3$ reveals a mass loss of 12.0 wt% at 125 °C. The temperature of the maximum NH_3 emission of the first step is at 62 °C for $Dy(BH_4)_3 \cdot 7NH_3$, which is 78 °C for $Gd(BH_4)_3 \cdot 7NH_3$ [119].

4.5. Binary metal ammine borohydides including $LiBH_4$ (Li-$M(BH_4)_x \cdot yNH_3$ (M = Al, Mg, Sc, Ti, Fe and Mn))

4.5.1. Synthesis

The $LiAl(BH_4)_4 \cdot 6NH_3$ can be obtained by mechanically milled the $Al(BH_4)_3 \cdot 6NH_3$ and $LiBH_4$ with a ratio of 1:1 for 60 min in argon atmosphere. It is a novel structure formed by $[Li_2(BH_4)_5]^{3-}$ and $[Al(NH_3)_6]^{3+}$ [130].

Similar with that of $LiAl(BH_4)_4 \cdot 6NH_3$, $LiMg(BH_4)_3 \cdot 2NH_3$ is obtained by ball-milling of $LiBH_4 \cdot NH_3$ and $Mg(BH_4)_2$ with a molar ratio of 2:1 at 350 rpm for 6 h [128].

$Li_2Mg(BH_4)_4 \cdot 6NH_3$ is another binary metal ammine borohydrides composited with Li^+ and Mg^{2+}, for which $Mg(BH_4)_2$ is first synthesized via a metathesis reaction between $Na(BH_4)$ and $MgCl_2$ in diethyl ether. Then $Mg(BH_4)_2 \cdot 6NH_3$ is obtained by ball milling $Mg(BH_4)_2$ under 6 bar of NH_3 atmosphere. Finally, the mixture of $Mg(BH_4)_2 \cdot 6NH_3$ and $LiBH_4$ with the ratio of 1:2 is ball milled at 500 rpm for 24 h to generate $Li_2Mg(BH_4)_4 \cdot 6NH_3$ [129].

$LiSc(BH_4)_4 \cdot 4NH_3$ is prepared by Yu's group in 2012. In the synthesis, $ScCl_3 \cdot 5NH_3$ was pre-fabricated by exposing $ScCl_3$ powder under 1 atm anhydrous ammonia at room temperature until its weight reached a constant. Then evacuation of $ScCl_3 \cdot 5NH_3$ at 100 °C for 0.5 h is to obtain $ScCl_3 \cdot 4NH_3$. Finally, $LiSc(BH_4)_4 \cdot 4NH_3$ is synthesized by ball-milling the mixture of $LiBH_4$ and $ScCl_3 \cdot 4NH_3$ with the molar ratio of 4:1 [123].

Additionally, $Li_2Ti(BH_4)_5 \cdot 5NH_3$ is prepared by ball milling the mixture of $TiCl_3 \cdot 5NH_3$ and $LiBH_4$ with the molar ratio of 1:4. After the decomposition, the regeneration by the direct reaction of the decomposed product with hydrazine and liquid ammonia was conducted in a sealed pressure vessel at 40 °C for 72 h, which appears an incomplete reduction of B-N bonds [121].

$Li_2Fe(BH_4)_4 \cdot 6NH_3$ (or $[Fe(NH_3)_6](Li_2(BH_4)_4)$) was found as a byproduct in the synthesis of $Fe(BH_4)_2 \cdot 6NH_3$, which is formed by the reaction of $FeCl_2$ and $LiBH_4$ in $S(CH_3)_2$ with NH_3 gas and dried under vacuum at low temperature [124].

Similarly, $Li_2Mn(BH_4)_4 \cdot 6NH_3$ can be prepared by the mechanical reaction between $Mn(BH_4)_2 \cdot 6NH_3$ and $LiBH_4$ (as showed in Table 10) [122].

4.5.2. Decomposition

There are two steps in the decomposition of $LiAl(BH_4)_4 \cdot 6NH_3$, which are observed in 75–150 °C and 190–250 °C, where only a slight of ammonia contamination can be detected in the first step. More than 10 wt% hydrogen with the purity of 99% can be released at 110–120 °C [130].

$LiMg(BH_4)_3 \cdot 2NH_3$ starts to release hydrogen below 100 °C. A slight emission of hydrogen is first detected at 143.5 °C. Then there are two peaks of mass loss at 221 and 388.5 °C, respectively. It totally liberates 8 wt% hydrogen below 200 °C. There are two steps about the gas emission including 10.0 wt% H_2 mixed with NH_3 in the first step and 5.7 wt% pure hydrogen in the second step upon heating the sample to 500 °C. The hydrogen purity in the total process gas is 98.9% [128].

As for $Li_2Mg(BH_4)_4 \cdot 6NH_3$, there are three steps for the decomposition including one deammoniation step and two dehydrogenation steps. A total of 37.30 wt% weight loss is found in the heating process from room temperature to 600 °C. There are 11.02 units of hydrogen (11.1 wt%) and 3.07 units of ammonia released totally from a unit of $Li_2Mg(BH_4)_4 \cdot 6NH_3$ in the experiment [129].

As for $LiSc(BH_4)_4 \cdot 4NH_3$, a total emission of 15.0 wt% hydrogen is achievable from room temperature to 240 °C through two stages (80–130 °C and 130–240 °C) with a small amount of contamination of ammonia. The hydrogen purity is up to 99.1%. In addition, more than 8 wt% pure hydrogen is released under the temperature of 110 °C [123].

$Li_2Ti(BH_4)_5 \cdot 5NH_3$ starts to dehydrogenate at 75 °C. A total of 9 wt% pure hydrogen is released from this compound by heating the sample at 100 °C for 400 min. As a result, 15.8 wt% (of the total mass) pure hydrogen is released in the decomposition after heating the sample to 300 °C [121].

The decomposition of $Li_2Fe(BH_4)_4 \cdot 6NH_3$ is triggered by NH_3 liberation, where the emission of B_2H_6 can be suppressed by the intermediate reaction with NH_3. $Li_2Fe(BH_4)_4 \cdot 6NH_3$ appears the high hydrogen density of ~14 wt % H_2 and releases a mixture of hydrogen and NH_3 gas below 80 °C [124].

Based on the analysis of the decomposition of the mixtures of $Mn(BH_4)_2 \cdot 6NH_3$ (47.0 wt%) + $Mn(BH_4)_2 \cdot 3NH_3$ (31.5 wt %) + $Li_2Mn(BH_4)_4 \cdot 6NH_3$ (21.5 wt%), it releases ammonia and a small amount of hydrogen at 60–100 °C (Table 10). As for another mixture of $Mn(BH_4)_2 \cdot 3NH_3$ (75.7 wt%) + $Li_2Mn(BH_4)_4 \cdot 6NH_3$ (20.7 wt%) + $Mn(BH_4)_2 \cdot 6NH_3$ (2.4 wt%), $Mn(BH_4)_2 \cdot 2NH_3$ (1.3 wt%), a total of 12.6 wt% hydrogen is observed in $Li_2Mn(BH_4)_4 \cdot 6NH_3$

(20.7 wt%), which first releases *ca.*1 equiv. NH_3 from 50 to 115 °C (Table 10). Then another 13 wt% mass is lost at 115–155 °C [122].

4.5.3. Theoretical analysis

The DFT calculation of Li-$M(BH_4)_x \cdot yNH_3$ indicates that the electron density is strongly localized around the BH_4 and NH_3 units, which suggests predominant covalent characters of the NH and BH bonds. The partial covalent bonding between Mg and the NH_3 units play an important role in the suppression of NH_3 emission during decomposition [128]. The removal enthalpies of ammonia and borane for $LiMg(BH_4)_3 \cdot 2NH_3$ is positive 112.02 kJ/mol and 37.6 kJ/mol, which indicates the excellent properties of dehydrogenation. For $LiCa(BH_4)_3 \cdot 2NH_3$ and $Li_2Al(BH_4)_5 \cdot 6NH_3$, the removal enthalpies of ammonia and borane are 51.0/259.16 and 116.20/247.46 kJ/mol [84]. From the comparison of the decomposition mechanisms of $LiBH_4NH_3$, $Mg(BH_4)_2(NH_3)_2$ and $LiMg(BH_4)_3 \cdot 2NH_3$ by using the CPMD simulation, the pure hydrogen is first generated between free hydrogen ions but not through the traditional dihydrogen bond of $H_2N\text{-}H^{\delta+} \cdots {}^{\delta-}H\text{-}BH_3$ [148]. Except the dopant of Li-$M(BH_4)_x \cdot yNH_3$, another series of binary metal ammine borohydides including $LiNH_2$ ($M(BH_4)_n$- $LiNH_2$, n = 1 or 2, M = Ca, Mg, Li) should be noted, which were synthesized by liquid ball milling. The metal in $M(BH_4)_n$-$4LiNH_2$ (M = Ca, Mg) samples not only facilitates the interaction of $[BH_4]^-$ and $[NH_2]^-$ groups, but also restrains the NH_3 release and slightly decreases the onset dehydrogenation temperature [149].

4.6. Binary metal ammine borohydrides with Na-Zn and V-Mg

4.6.1. Synthesis

$NaZn(BH_4)_3$ is first prepared by ball milling the mixture of $NaBH_4$ and $ZnCl_2$ with the molar ratio of 3:1 for 15 h in an argon atmosphere. Then $NaZn(BH_4)_3 \cdot 2NH_3$ is synthesized by introducing anhydrous ammonia into the as-prepared $NaZn(BH_4)_3$ in ether around 0 °C. The mixture of $NaZn(BH_4)_3 \cdot 2NH_3$-$NaZn(BH_4)_3$ is synthesized by ball-milling the two components for 10–30 min with a ratio of 1:1 in argon [150].

$VMg(BH_4)_5 \cdot 5NH_3$ is obtained by ball-milled $Mg(BH_4)_2$ and the prepared $V(BH_4)_3 \cdot 5NH_3$ [123] with agitation frequency of 280 rpm with the molar ratio of 1:1 [131].

4.6.2. Decomposition

$NaZn(BH_4)_3 \cdot 2NH_3$ generates 118 mL/g hydrogen in 5 min and 992 mL/g hydrogen in 2 h with the energy barrier of 56.9 kJ/mol. The mixture of $NaZn(BH_4)_3 \cdot 2NH_3$ generates 717 mL/g hydrogen in 5 min and 1643 mL/g in 2 h with the activation energy of 32.5 kJ/mol. The slight ammonia liberation can be found in both the two processes [150].

$VMg(BH_4)_5 \cdot 5NH_3$ starts to release hydrogen at 65 °C. It releases over 10 wt% pure hydrogen without any undesirable byproducts. At 160 °C, the hydrogen release is completed within 50 min with the capacity of 9.9 wt% H_2. For the sample held at 100 °C, 120 °C and 150 °C, about 7.9 wt%, 8.2 wt% and 9.7 wt% H_2 are generated in 500 min, respectively [131].

4.7. Ternary ammine borohydrides with Cr-Li-$ZnCl_2$

$CrCl_3 \cdot 5NH_3$ is first synthesized by reacting $CrCl_3$ with NH_3 in liquid ammonia, which is annealed at 220 °C for 5 min and 300 °C for 10 min to obtain $CrCl_3 \cdot 3NH_3$. Then the ball-milled $CrCl_3 \cdot 3NH_3$-$3LiBH_4$ releases hydrogen in the temperature range of 100–170 °C with the purity of 91.8 wt% (slightly contaminated with ammonia). Further improvement on the dehydrogenation of $CrCl_3 \cdot 3NH_3$-$3LiBH_4$ is conducted by the addition of $ZnCl_2$. The 0.5 mol $ZnCl_2$

Table 11
The dehydrogenation properties of AMBs.

Compound	Radius of center ions (Å)	Electroegativity of center ions	H content (Theor wt%)	H content (Exp wt% with the Temp)	Byproducts
$LiBH_4 \cdot NH_3$ [114]	0.76	14.59	18.06	4.0 wt% (280 °C)	NH_3
$2LiBH_4 \cdot NH_3$ - $MgCl_2$ [132]	Li/Mg: 0.72/0.76	17.13/14.59	8.12	7.0 wt% (241 °C)	NH_3 (slightly)
$2LiBH_4 \cdot NH_3$ - $ZnCl_2$ [132]	Li/Zn: 0.74/0.76	10.38/14.59	6.56	5.6 wt (129 °C)	NH_3
$5LiBH_4 \cdot NH_3$ - $AlCl_3$ [132]	Li/Al: 0.54/0.76	26.72/14.59	10.70	9.1 wt% (145 °C)	NH_3
$LiBH_4 \cdot NH_3$- ($3LiH\text{-}3NH_3BH_3$) [134]	0.76	14.59	18.06	10 wt% (100 °C)	None
$Mg(BH_4)_2 \cdot 2NH_3$ [115]	0.72	17.13	15.98	13.1 wt% (400 °C) 14.9 wt% (500 °C)	None
Nano-$Mg(BH_4)_2 \cdot 6NH_3$ [138]	0.72	17.13	16.71	14.5 wt% (450 °C)	NH_3 (29%)
$Mg(BH_4)_2 \cdot 2NH_3$ -$LiBF_4$ [139]	Mg/Li: 0.72/0.76	17.13	–	9.21 wt% (150 °C)	None
$Mg(BH_4)_2 \cdot 2NH_3$ -$2NaAlH_4$ [141]	Mg/Na/Al:0.72/1.02/0.54	17.13/9.44/26.72	13.36	11.3 wt% (70 °C)	None
$Al(BH_4)_3 \cdot 6NH_3$ [144]	0.54	26.72	17.30	12 wt% (120 °C)	None
$Ca(BH_4)_2 \cdot NH_3$ [116]	1.00	11.30	12.70	12 wt% (250 °C)	None
$Ca(BH_4)_2 \cdot 2\ NH_3$ [117]	1.00	11.30	13.51	11.3 wt% (500 °C)	None
$Ca(BH_4)_2 \cdot NH_3$-$LiBH_4$	Ca/Li: 1.00/0.76	11.30/14.59	13.84	12.1 wt% (250 °C)	None
$Ca(BH_4)_2 \cdot 4NH_3$ - $Mg(BH_4)_2$ [143]	Ca/Mg: 1.00/0.72	11.30/17.13	14.64	9 wt% (62 °C)	NH_3 (slightly)
$Y(BH_4)_3 \cdot 4NH_3$ [119]	0.9(III)	14.82(III)	11.92	8.7 wt% (200 °C)	None
$Ti(BH_4)_3 \cdot 5NH_3$ [121]	0.67(III)	12.74(III)	15.23	13.4 wt% (200 °C)	NH_3 (slightly)
$Ti(BH_4)_3 \cdot 3NH_3$ [121]	0.67(III)	12.74(III)	14.65	14 wt% (300 °C)	None
$V(BH_4)_3 \cdot 5NH_3$ [123]	0.61	13.68	14.97	11.5 wt% (400 °C)	NH_3
$V(BH_4)_3 \cdot 3NH_3$ [123]	0.61	13.68	14.35	14.3 wt% (300 °C)	None
$Fe(BH_4)_2 \cdot 6NH_3$ [124]	0.61(II)	8.43(II)	13.87	–	NH_3 (mainly)
$Zn(BH_4)_3 \cdot 2NH_3$ [125]	0.74	10.38	12.55	8.9 wt% (115 °C)	None
$Sr(BH_4)_2 \cdot 4NH_3$ [126]	1.18	9.83	10.80		NH_3 (mainly)
$Zr(BH_4)_4 \cdot 8NH_3$ [127]	0.72	10.32	13.96	8.5 wt% (150 °C)	NH_3
$NbCl_5 \cdot 5NH_3$-$5LiBH_4$	Nb/Li: 0.64/0.76	11.40/14.59	7.54	11.2 wt% (250 °C)	None
$Gd(BH_4)_3 \cdot 7NH_3$ [119]	0.938	–	10.29	19.5 wt% mixture	NH_3 (mainly)
$Dy(BH_4)_3 \cdot 7NH_3$ [119]	0.912	–	10.12	12.0 wt% mixture	NH_3 (mainly)
$Li_2Al(BH_4)_5 \cdot 6NH_3$ [130]	Li/Al: 0.76/0.54	14.59/26.72	17.52	10 wt% (250 °C)	NH_3
$LiMg(BH_4)_3 \cdot 2NH_3$ [128]	Li/Mg: 0.76/0.72	14.59/17.13	16.46	8 wt% (200 °C)	NH_3
$Li_2Mg(BH_4)_4 \cdot 6NH_3$ [129]	Li/Mg: 0.76/0.72	14.59/17.13	17.08	11.1 wt% (600 °C)	NH_3
$LiSc(BH_4)_4 \cdot 4NH_3$ [123]	Li/Sc: 0.76/0.745(III)	14.59/17.68(III)	15.63	15.1 wt% (300 °C)	None
$Li_2Ti(BH_4)_5 \cdot 5NH_3$ [121]	Li/Ti: 0.76/0.67(III)	14.59/12.74(III)	15.85	15.8 wt% (300 °C)	None
$Li_2Fe(BH_4)_4 \cdot 6NH_3$ [124]	Li/Fe: 0.76/0.78(II)	14.59/8.43(II)	14.71	14 wt% (80 °C)	NH_3
$Li_2Mn(BH_4)_4 \cdot 6NH_3$ [122]	Li/Mn: 0.76/0.67(III)	14.59/8.88(II)	14.78	12.6 wt% (155 °C)	NH_3
$VMg(BH_4)_5 \cdot 5NH_3$ [131]	V(III)/Mg: 0.61/0.72	13.68(III)/17.13	14.96	10 wt% (65 °C)	None

assisted sample is able to release 7.4 wt% of hydrogen with the purity of 98.8 mol% [151].

4.8. Summary

AMBs are prepared by directly ball milling metal borohydrides and water-free ammonia generally. The dehydrogenation performances are dominated by the stability of metal borohydrides in AMBs. It releases hydrogen only when the stability of AMB is larger than that of the corresponding metal borohydrides, otherwise, it releases ammonia. The stabilization is due to the complex formation in ammine metal borohydrides with high electronegativities ($Xp > 1.6$), causing a shielding effect to the metal cation [33]. Based on our CPMD study, some AMBs liberates ammonia at low temperature but releases hydrogen at high temperature, such as $LiBH_4 \cdot nNH_3$, which is caused by M – N intensive vibration at low temperature and hydrogen radical combinations at high temperature [135,152]. Compared with the monometallic AMBs, the structure of the multi metal amine borohydrides is combined by two parts of MBH_4 and $M'NH_3$, where the $[MBH_4]$ group can favour the formation of $H^{\delta+}$, and improve the efficiency of dehydrogenation process and purity of released hydrogen from bimetallic ammine borohydrides (AMBs), which is due to the different bond strength of M – B and M – N bonds [84]. We summarized the dehydrogenation performances of different kinds of AMBs as Table 11.

5. Future perspectives

Over the past decades, it is an extremely fast development including the synthesis methods for diverse new MBNH materials, application experiments and theoretical study about the controllable hydrogenation and dehydrogenation.

In this field, the hydrogen content and purity of MBNH materials can be enhanced by developing the multi metals to control the hydrogen-storage anions or groups with high H contents such as $[BH_4]^-$, N_2H_4 or NH_3. Commonly, all these compounds release hydrogen through the different hydrogen resources of H(N) and H(B). Whether the mono metal or multi metals in the system, they interact with B atom through electrostatic relationship and with N atom through coordination bonds. In the decomposition, metal in MBNH compound is generally as a hydrogen carrier to catalyse the formation of the dihydrogen bond. The dehydrogenation performances of MBNH are mainly dominated by the polarity of metal or metal-metal interaction.

However, the classic problem about the reversibility is partly resolved by introducing N_2H_4 or Frustrated Lewis Pairs (FLPs). N_2H_4 had been proved effective to convert $[BNH_2]$ to BH_3NH_3 as a nearly thermo neutral reaction. As for the Frustrated Lewis Pairs, it is very attractive in activating the small molecules including H_2, by using the very active chemical properties for splitting traditional Lewis Pairs. The problem in this field should be centred on the controllability of synthesis from a designed target. MBNH materials are composited by some very simple groups of NH_3, BH_4, $NH_2BH_3^-$, NH_2^- and $NHNH_2BH_3^-$. Whether using the additional hydrazine or introducing the 'FLPs' in to MBNH systems, all the compounds or groups can be seen as the material genes, we need to combine them with different metals for the better MBNH hydrogen storage performances.

Acknowledgements

This work was partially supported by the National Science Fund for Distinguished Young Scholars (51625102), the National Natural Science Foundation of China (21701001), the Innovation Program of Shanghai Municipal Education Commission (2019-01-07-00-07-E00028), the Science and Technology Commission of Shanghai Municipality (Grant No. 17XD1400700), the Anhui Provincial Natural Science Foundation (1708085QB42) and the China Postdoctoral Science Foundation (2018M632013).

References

[1] United States Department of Energy, Targets for Onboard Hydrogen Storage Systems for Light-Duty Vehicles, 2009.
[2] N.L. Rosi, J. Eckert, M. Eddaoudi, D.T. Vodak, J. Kim, M. O'Keeffe, O.M. Yaghi, Hydrogen storage in microporous metal-organic frameworks, Science 300 (2003) 1127–1129.
[3] H. Furukawa, K.E. Cordova, M. O'Keeffe, O.M. Yaghi, The chemistry and applications of metal-organic frameworks, Science 341 (2013) 974–986.
[4] A. Ahmed, Y. Liu, J. Purewal, L.D. Tran, A.G. Wong-Foy, M. Veenstra, A.J. Matzger, D.J. Siegel, Balancing gravimetric and volumetric hydrogen density in MOFs, Energy Environ. Sci. 10 (2017) 2459–2471.
[5] A.C. Dillon, K.M. Jones, T.A. Bekkedahl, C.H. Kiang, D.S. Bethune, M.J. Heben, Storage of hydrogen in single-walled carbon nanotubes, Nature 386 (1997) 377–379.
[6] X.B. Yu, Z.W. Tang, D.L. Sun, L.Z. Ouyang, M. Zhu, Recent advances and remaining challenges of nanostructured materials for hydrogen storage applications, Prog. Mater. Sci. 88 (2017) 1–48.
[7] P. Chen, Z.T. Xiong, J.Z. Luo, J.Y. Lin, K.L. Tan, Interaction of hydrogen with metal nitrides and imides, Nature 420 (2002) 302–304.
[8] J. Yang, X. Wang, J. Mao, L. Chen, H. Pan, S. Li, H. Ge, C. Chen, Investigation on reversible hydrogen storage properties of $Li_3AlH_6/2LiNH_2$ composite, J. Alloys Compd. 494 (2010) 58–61.
[9] J. Mao, Z. Guo, X. Yu, M. Ismail, H. Liu, Enhanced hydrogen storage performance of $LiAlH_4$-MgH_2-TiF_3 composite, Int. J. Hydrogen Energy 36 (2011) 5369–5374.
[10] Y. Liu, H. Pan, M. Gao, Q. Wang, Advanced hydrogen storage alloys for Ni/MH rechargeable batteries, J. Mater. Chem. 21 (2011) 4743–4756.
[11] B. Liao, Y.Q. Lei, L.X. Chen, G.L. Lu, H.G. Pan, Q.D. Wang, A study on the structure and electrochemical properties of $La_2Mg(Ni_{0.95}M_{0.05})_9$ (M = Co, Mn, Fe, Al, Cu, Sn) hydrogen storage electrode alloys, J. Alloys Compd. 376 (2004) 186–195.
[12] H. Pan, Y. Liu, M. Gao, Y. Zhu, Y. Lei, Q. Wang, An investigation on the structural and electrochemical properties of $La_{0.7}Mg_{0.3}(Ni_{0.85}Co_{0.15})_x$ (x=3.15–3.80) hydrogen storage electrode alloys, J. Alloys Compd. 351 (2003) 228–234.
[13] Y. Liu, H. Pan, M. Gao, Y. Zhu, Y. Lei, Q. Wang, The effect of Mn substitution for Ni on the structural and electrochemical properties of $La_{0.7}Mg_{0.3}Ni_{2.55-x}Co_{0.45}Mn_x$ hydrogen storage electrode alloys, Int. J. Hydrogen Energy 29 (2004) 297–305.
[14] B. Liao, Y.Q. Lei, L.X. Chen, G.L. Lu, H.G. Pan, Q.D. Wang, Effect of the La/Mg ratio on the structure and electrochemical properties of $LaxMg_{3-x}Ni_9$ (x = 1.6–2.2) hydrogen storage electrode alloys for nickel–metal hydride batteries, J. Power Sources 129 (2004) 358–367.
[15] B. Liao, Y.Q. Lei, G.L. Lu, L.X. Chen, H.G. Pan, Q.D. Wang, The electrochemical properties of $La_xMg_{3-x}Ni_9$ (x = 1.0-2.0) hydrogen storage alloys, J. Alloys Compd. 356–357 (2003) 746–749.
[16] H. Pan, Y. Liu, M. Gao, Y. Zhu, Y. Lei, The structural and electrochemical properties of $La_{0.7}Mg_{0.3}(Ni_{0.85}Co_{0.15})_x$ (x = 3:0–5.0) hydrogen storage alloys, Int. J. Hydrogen Energy 28 (2003) 1219–1228.
[17] A. Staubitz, A.P.M. Robertson, I. Manners, Ammonia-borane and related compounds as dihydrogen sources, Chem. Rev. 110 (2010) 4079–4124.
[18] T.E. Stennett, S. Harder, s-Block amidoboranes: syntheses, structures, reactivity and applications, Chem. Soc. Rev. 45 (2015) 1112–1118.
[19] T. He, P. Pachfule, H. Wu, Q. Xu, P. Chen, Hydrogen carriers, Nat. Rev. Mater. 1 (2016) 1–17.
[20] Y. Liu, K. Zhong, K. Luo, M. Gao, H. Pan, Q. Wang, Size-dependent kinetic enhancement in hydrogen absorption and desorption of the Li-Mg-N-H system, J. Am. Chem. Soc. 131 (2009) 1862–1870.
[21] M.J. Valero-Pedraza, D. Cot, E. Petit, K.F. Aguey-Zinsou, J.G. Alauzun, U.B. Demirci, Ammonia borane nanospheres for hydrogen storage, ACS Appl. Nano Mater. 2 (2019) 1129–1138.
[22] L.B. Diaz, J.M. Hanlon, M. Bielewski, A. Milewska, D.H. Gregory, Ammonia borane based nanocomposites as solid-state hydrogen stores for portable power applications, Energy Technol. 6 (2018) 583–594.
[23] A. Lale, S. Bernard, U.B. Demirci, Boron nitride for hydrogen storage, ChemplusChem 83 (2018) 893–903.
[24] J.F. Petit, U.B. Demirci, Mechanistic insights into dehydrogenation of partially deuterated ammonia borane NH_3BD_3 being heating to 200 °C, Inorg. Chem. 58 (2019) 489–494.
[25] S.G. Shore, R.W. Parry, The crystalline compound ammonia-borane, H_3NBH_3, J. Am. Chem. Soc. 77 (1955) 6084–6085.
[26] V. Rizzi, D. Polino, E. Sicilia, N. Russo, M. Parrinello, The onset of dehydrogenation in solid ammonia borane: an ab initio metadynamics study, Angew. Chem. Int. Ed. 131 (2019) 4016–4020.
[27] S.S. Wise, J.L. Margrave, H.M. Feder, W.N. Hubbard, Fluorine bomb calorimetry. XVI. The enthalpy of formation of boron nitride, J. Phys. Chem. 70 (1966) 7–10.

[28] R. Moury, U.B. Demirci, Hydrazine borane and hydrazinidoboranes as chemical hydrogen storage materials, Energies 8 (2015) 3118–3141.
[29] S. Pylypko, E. Petit, P.G. Yot, F. Salles, M. Cretin, P. Miele, U.B. Demirci, Key study on the potential of hydrazine bisborane for solid- and liquid- state chemical hydrogen storage, Inorg. Chem. 54 (2015) 4574–4583.
[30] C. Wan, L. Sun, L. Xu, D. Cheng, F. Chen, X. Zhan, Y. Yang, Novel NiPt alloy nanoparticle decorated 2D layered g-C3N4 nanosheets: a highly efficient catalyst for hydrogen generation from hydrous hydrazine, J. Mater. Chem. A 7 (2019) 8798–8804.
[31] Y. Lin, L. Yang, H. Jiang, Y. Zhang, D. Cao, C. Wu, G. Zhang, J. Jiang, L. Song, Boosted reactivity of ammonia borane dehydrogenation over Ni/Ni_2P heterostructure, J. Phys. Chem. Lett. 10 (2019) 1048–1054.
[32] A. Züttel, P. Wenger, S. Rentsch, P. Sudan, Ph. Mauron, Ch. Emmenegger, $LiBH_4$ a new hydrogen storage material, J. Power Sources 118 (2003) 1–7.
[33] M. Paskevicius, L.H. Jepsen, P. Schouwink, R. Cèrny, D.B. Ravnsbæk, Y. Filinchuk, M. Dornheim, F. Besenbacher, T.R. Jensen, Metal borohydrides and derivatives–synthesis, structure and properties, Chem. Soc. Rev. 46 (2017) 1565–1634.
[34] Himashinie V.K. Diyabalanage, Roshan P. Shrestha, Troy A. Semelsberger, Brian L. Scott, Mark E. Bowden, Benjamin L. Davis, A.K. Burrell, Calcium amidotrihydroborate: a hydrogen storage material, Angew. Chem. Int. Ed. 46 (2007) 8995–8997.
[35] Z.T. Xiong, C.K. Yong, G.T. Wu, P. Chen, W. Shaw, A. Karkamkar, T. Autrey, M.O. Jones, S.R. Johnson, P.P. Edwards, W.I.F. David, High-capacity hydrogen storage in lithium and sodium amidoboranes, Nat. Mater. 7 (2008) 138–141.
[36] B.C. Filiz, A.K. Figen, S. Pişkin, Dual combining transition metal hybrid nanoparticles for ammonia borane hydrolytic dehydrogenation, Appl. Catal. A Gen. 550 (2018) 320–330.
[37] Shin-ichi Orimo, Yuko Nakamori, Jennifer R. Eliseo, Andreas Züttel, C.M. Jensen, Complex hydrides for hydrogen storage, Chem. Rev. 107 (2007) 4111–4132.
[38] K.R. Graham, T. Kemmitt, M.E. Bowden, High capacity hydrogen storage in a hybrid ammonia borane–lithium amide material, Energy Environ. Sci. 2 (2009) 706–710.
[39] G.L. Xia, X.B. Yu, Y.H. Guo, Z. Wu, C.Z. Yang, H.K. Liu, S.X. Dou, Amminelithium amidoborane Li(NH_3)NH_2BH_3: a new coordination compound with favorable dehydrogenation characteristics, Chem. Eur. J. 16 (2010) 3763–3769.
[40] Ping Chen, Zhitao Xiong, Jizhong Luo, Jianyi Lin, K.L. Tan, Interaction of hydrogen with metal nitrides and imides, Nature 420 (2002) 302–304.
[41] Yuko Nakamori, S. Orimo, Destabilization of Li-based complex hydrides, J. Alloys Compd. 365 (2004) 271–275.
[42] H. Wu, W. Zhou, T. Yildirim, Alkali and alkaline-earth metal amidoboranes: structure, crystal chemistry, and hydrogen storage properties, J. Am. Chem. Soc. 130 (2008) 14834–14839.
[43] Y. Zhang, K. Shimoda, T. Ichikawa, Y. Kojima, Activation of ammonia borane hybridized with alkaline-metal hydrides: a low-temperature and high-purity hydrogen generation material, J. Phys. Chem. C 114 (2010) 14662–14664.
[44] K. Wang, J.G. Zhang, T.-T. Man, M. Wu, C.C. Chen, Recent process and development of metal aminoborane, Chem. Asian J. 8 (2013) 1076–1089.
[45] C.Z. Wu, G.T. Wu, Z.T. Xiong, W.I.F. David, K.R. Ryan, M.O. Jones, P.P. Edwards, H.L. Chu, P. Chen, Stepwise phase transition in the formation of lithium amidoborane, Inorg. Chem. 49 (2010) 4319–4323.
[46] C. Wu, G. Wu, Z. Xiong, X. Han, H. Chu, T. He, P. Chen, $LiNH_2BH_3 \cdot 3NH_3BH_3$: structure and hydrogen storage properties, Chem. Mater. 22 (2010) 3–5.
[47] H.V.K. Diyabalanage, T. Nakagawa, R.P. Shrestha, T.A. Semelsberger, B.L. Davis, B.L. Scott, A.K. Burrell, W.I.F. David, K.R. Ryan, M.O. Jones, P.P. Edwards, Potassium(I) amidotrihydroborate: structure and hydrogen release, J. Am. Chem. Soc. 132 (2010) 11836–11837.
[48] Y.S. Chua, G.T. Wu, Z.T. Xiong, A. Karkamkar, J.P. Guo, M.X. Jian, M.W. Wong, T. Autrey, P. Chen, Synthesis, structure and dehydrogenation of magnesium amidoborane monoammoniate, Chem. Commun. 46 (2010) 5752–5754.
[49] J.H. Luo, X.D. Kang, Z.Z. Fang, P. Wang, Promotion of hydrogen release from ammonia borane with magnesium nitride, Dalton Trans. 40 (2011) 6469–6474.
[50] Z.T. Xiong, G.T. Wu, J.J. Hu, P. Chen, Ca–Na–N–H system for reversible hydrogen storage, J. Alloys Compd. 141 (2007) 152–156.
[51] Q.A. Zhang, C.X. Tang, C.H. Fang, F. Fang, D. Sun, L.Z. Ouyang, M. Zhu, Synthesis, crystal structure, and thermal decomposition of strontium amidoborane, J. Phys. Chem. C 114 (2010) 1709–1714.
[52] K. Wang, V. Arcisauskaite, J.S. Jiao, J.G. Zhang, T.L. Zhang, Z.N. Zhou, Structural prediction, analysis and decomposition mechanism of solid M$(NH_2BH_3)_n$ (M=Mg, Ca and Al), RSC Adv. 4 (2014) 14624–14632.
[53] R.V. Genova, K.J. Fijalkowski, A. Budzianowski, W. Grochala, Towards Y$(NH_2BH_3)_3$: probing hydrogen storage properties of YX_3/MNH_2BH_3 (X = F, Cl; M = Li, Na) and YH_{x-3}/NH_3BH_3 composites, J. Alloys Compd. 499 (2010) 144–148.
[54] A.G. Myers, B.H. Yang, K.J. David, Lithium amidotrihydroborate, a powerful new reductant. Transformation of tertiary amides to primary alcohols, Tetrahedron Lett. 37 (1996) 3623–3626.
[55] Z. Xiong, Y. Chua, G. Wu, L. Wang, M.W. Wong, Z.M. Kam, T. Autrey, T. Kemmittd, P. Chen, Interaction of ammonia borane with Li_2NH and Li_3N, Dalton Trans. 39 (2010) 720–722.
[56] H.I. Schlesinger, A.B. Burg, Hydrides of boron. VIII. The structure of the diammoniate of diborane and its relation to the structure of diborane, J. Am. Chem. Soc. 60 (1938) 290–299.
[57] F.P.R. Sandra, U.B. Demirci, R. Chiriac, R. Moury, P. Miele, A simple preparation method of sodium amidoborane, highly efficient derivative of ammonia borane dehydrogenating at low temperature, Int. J. Hydrogen Energy 36 (2011) 7423–7430.
[58] Z. Xiong, G. Wu, Y.S. Chua, J. Hu, T. He, W. Xu, P. Chen, Synthesis of sodium amidoborane ($NaNH_2BH_3$) for hydrogen production, Energy Environ. Sci. 1 (2008) 360–363.
[59] K.R. Ryan, A.J. Ramirez-Cuesta, K. Refson, M.O. Jones, P.P. Edwards, W.I.F. David, A combined experimental inelastic neutron scattering, Raman and ab initio lattice dynamics study of alpha-lithium amidoborane, Phys. Chem. Chem. Phys. 13 (2011) 12249–12253.
[60] S. Bhattacharya, Z. Xiong, G. Wu, P. Chen, Y.P. Feng, C. Majumder, G.P. Das, Dehydrogenation mechanism of monoammoniated lithium amidoborane [Li(NH_3)NH_2BH_3], J. Phys. Chem. C 116 (2012) 8859–8864.
[61] D.P. Kim, K.T. Moon, J.G. Kho, J. Economy, C. Gervais, F. Babonneau, Synthesis and characterization of poly-(aminoborane) as a new boron nitride precursor, Polym. Adv. Technol. 10 (1999) 702–712.
[62] T.A. Luedtke, T. Autrey, Hydrogen release studies of alkali metal amidoboranes, Inorg. Chem. 49 (2010) 3905–3910.
[63] K.J. Fijakowski, W. Grochala, Substantial emission of NH_3 during thermal decomposition of sodium amidoborane, $NaNH_2BH_3$, J. Mater. Chem. 19 (2009) 2043–2050.
[64] K. Shimoda, Y. Zhang, T. Ichikawa, H. Miyaoka, Y. Kojima, Solid state NMR study on the thermal decomposition pathway of sodium amidoborane $NaNH_2BH_3$, J. Mater. Chem. 21 (2011) 2609–2615.
[65] K. Shimoda, K. Doi, T. Nakagawa, Y. Zhang, H. Miyaoka, T. Ichikawa, Masataka Tansho, T. Shimizu, A.K. Burrel, Y. Kojima, Comparative study of structural changes in NH_3BH_3, $LiNH_2BH_3$, and KNH_2BH_3 during dehydrogenation process, J. Phys. Chem. C 116 (2012) 5957–5964.
[66] S.A. Shevlin, B. Kerkeni, Z.X. Guo, Dehydrogenation mechanisms and thermodynamics of MNH_2BH_3 (M = Li, Na) metal amidoboranes as predicted from first principles, Phys. Chem. Chem. Phys. 13 (2011) 7649–7659.
[67] T.B. Lee, M.L. McKee, Mechanistic study of $LiNH_2BH_3$ formation from $(LiH)_4 + NH_3BH_3$ and subsequent dehydrogenation, Inorg. Chem. 48 (2009) 7564–7575.
[68] S. Swinnen, V.S. Nguyen, M.T. Nguyen, Theoretical study of the hydrogen release mechanism from a lithium derivative of ammonia borane, $LiNH_2BH_3$–NH_3BH_3, Chem. Phys. Lett. 517 (2011) 22–28.
[69] W. Li, R.H. Scheicher, C.M. Araujo, G.T. Wu, A. Blomqvist, C.Z. Wu, R. Ahuja, Y.P. Feng, P. Chen, Understanding from first-principles why $LiNH_2BH_3 \cdot NH_3BH_3$ shows improved dehydrogenation over $LiNH_2BH_3$ and NH_3BH_3, J. Phys. Chem. C 114 (2010) 19089–19095.
[70] J. Luo, X. Kang, P. Wang, Synthesis, formation mechanism, and dehydrogenation properties of the long-sought Mg$(NH_2BH_3)_2$ compound, Energy Environ. Sci. 6 (2013) 1018–1025.
[71] Y.S. Zhang, C. Wolverton, Crystal structures, phase stabilities, and hydrogen storage properties of metal amidoboranes, J. Phys. Chem. C 116 (2012) 14224–14231.
[72] Y.S. Chua, H. Wu, W. Zhou, T.J. Udovic, G.T. Wu, Z.T. Xiong, M.W. Wong, P. Chen, Monoammoniate of calcium amidoborane: synthesis, structure, and hydrogen-storage properties, Inorg. Chem. 51 (2012) 1599–1603.
[73] Y.S. Chua, G.T. Wu, Z.T. Xiong, T. He, P. Chen, Calcium amidoborane ammoniate-synthesis, structure, and hydrogen storage properties, Chem. Mater. 21 (2009) 4899–4904.
[74] Y. Zhang, K. Shimoda, H. Miyaoka, T. Ichikawa, Y. Kojima, Thermal decomposition of alkaline-earth metal hydride and ammonia borane composites, Int. J. Hydrogen Energy 35 (2010) 12405–12409.
[75] C.B. Lingam, K.R. Babu, S.P. Tewari, G. Vaitheeswaran, S. Lebegue, Electronic structure and optical properties of Ca$(NH_2BH_3)_2$ studied from GW calculations, J. Phys. Chem. C 115 (2011) 18795–18801.
[76] S. Harder, J. Spielmann, B. Tobey, Calcium–amidoborane–ammine complexes: thermal decomposition of model systems, Chem. Eur. J. 18 (2012) 1984–1991.
[77] W. Li, G. Wu, Y. Chua, Y.P. Feng, P. Chen, Role of NH_3 in the dehydrogenation of calcium amidoborane ammoniate and magnesium amidoborane ammoniate: a first-principles study, Inorg. Chem. 51 (2011) 76–87.
[78] S.S. Jalisatgi, J.G. Wu, M.F. Hawthorne, Chemical Hydrogen Storage Using Aluminum Ammonia-Borane Complexes, University of Missouri–Columbia, 2009.
[79] J. Yang, P.R. Beaumont, T.D. Humphries, C.M. Jensen, X. Li, Efficient synthesis of an aluminum amidoborane ammoniate, Energies 8 (2015) 9107–9116.
[80] T. Jarón, W. Grochala, Y$(BH_4)_3$—an old–new ternary hydrogen store aka learning from a multitude of failures, Dalton Trans. 39 (2010) 160–166.
[81] M.F. Hawthorne, S.S. Jalisatgi, J. Wu, Chemical Hydrogen Storage Using Polyhedral Borane Anions and Aluminum-Ammonia-Borane Complexes, Annual Progress Report, 2009.
[82] M.F. Hawthorne, S.S. Jalisatgi, H.B. Lee, J. Wu, Chemical Hydrogen Storage Using Aluminum Ammonia-Borane Complexes, University of Missouri, 2010.
[83] K. Wang, J.-G. Zhang, T. Li, Y. Liu, T. Zhang, Z.N. Zhou, Electronic structures and dehydrogenation properties of bimetallic amidoboranes, Int. J. Hydrogen Energy 40 (2015) 2500–2508.
[84] K. Wang, J.G. Zhang, J.S. Jiao, T. Zhang, Z.N. Zhou, A first-principles study: structure and decomposition of mono-/bimetallic ammine borohydrides, J. Phys. Chem. C 118 (2014) 8271–8279.
[85] K.J. Fijalkowski, R.V. Genova, Y. Filinchuk, A. Budzianowski, M. Derzsi,

T. Jaron, P.J. Leszczynski, W. Grochala, Na[Li(NH_2BH_3)$_2$] - the first mixed-cation amidoborane with unusual crystal structure, Dalton Trans. 40 (2011) 4407–4413.
[86] X.D. Kang, J.H. Luo, Q.G. Zhang, P. Wang, Combined formation and decomposition of dual-metal amidoborane $NaMg(NH_2BH_3)_3$ for high-performance hydrogen storage, Dalton Trans. 40 (2011) 3799–3801.
[87] H. Wu, W. Zhou, F.E. Pinkerton, M.S. Meyer, Q.R. Yao, S. Gadipelli, T.J. Udovic, T. Yildirim, J.J. Rush, Sodium magnesium amidoborane: the first mixed-metal amidoborane, Chem. Commun. 47 (2011) 4102–4104.
[88] I. Dovgaliuk, L.H. Jepsen, D.A. Safin, Z. Łodziana, V. Dyadkin, T.R. Jensen, M. Devillers, Y. Filinchuk, A composite of complex and chemical hydrides yields the first Al-based amidoborane with improved hydrogen storage properties, Chem. Eur. J. 21 (2015) 14562–14570.
[89] K.T. Møller, M. Jørgensen, J.G. Andreasen, J. Skibsted, Z. Łodziana, Y. Filinchuk, T.R. Jensen, Synthesis and thermal decomposition of potassium tetraamidoboranealuminate, K[Al(NH_2BH_3)$_4$], Int. J. Hydrogen Energy 43 (2018) 311–321.
[90] Y.S. Chua, W. Li, G. Wu, Z. Xiong, P. Chen, From exothermic to endothermic dehydrogenation - interaction of monoammoniate of magnesium amidoborane and metal hydrides, Chem. Mater. 24 (2012) 3574–3581.
[91] B. Liu, Y.S. Chua, G.T. Wu, Z.T. Xiong, P. Chen, Synthesis and dehydrogenation of $LiCa(NH_2)_3(BH_3)_2$, Int. J. Hydrogen Energy 37 (2012) 9076–9081.
[92] W. Li, L. Miao, R.H. Scheicher, Z.T. Xiong, G.T. Wu, C.M. Araújo, A. Blomqvist, R. Ahuja, Y.P. Feng, P. Chen, Li–Na ternary amidoborane for hydrogen storage: experimental and first-principles study, Dalton Trans. 41 (2012) 4754–4764.
[93] K. Wang, J.G. Zhang, P. He, Theoretical study on the structure and dehydrogenation mechanism of mixed metal amidoborane, Na[Li(NH_2BH_3)]$_2$, J. Alloys Compd. 581 (2013) 59–65.
[94] K. Wang, J.G. Zhang, T.L. Zhang, Crystal and electronic structures of solid $M(NH_2BH_3)_n$ (M = Li, Na, K) and the decomposition mechanisms, Int. J. Hydrogen Energy 39 (2014) 21372–21379.
[95] K. Wang, J.G. Zhang, Structural study and dehydrogenation mechanisms of a novel mixed metal amidoborane: sodium magnesium amidoborane, Chem. Phys. Lett. 590 (2013) 27–34.
[96] A. Al-Kukhun, H.T. Hwang, A. Varma, Mechanistic studies of ammonia borane dehydrogenation, Int. J. Hydrogen Energy 38 (2013) 169–179.
[97] D.Y. Kim, N.J. Singh, H.M. Lee, K.S. Kim, Hydrogen-release mechanisms in lithium amidoboranes, Chem. Eur. J. 15 (2009) 5598–5604.
[98] W. Li, G. Wu, Y. Chua, Y.P. Feng, P. Chen, Role of NH_3 in the dehydrogenation of calcium amidoborane ammoniate and magnesium amidoborane ammoniate: a first principles study, Inorg. Chem. 51 (2012) 76–87.
[99] M. Ramzan, R. Ahuja, Hybrid density functional and molecular dynamics study of promising hydrogen storage materials: double metal amidoboranes and metal amidoborane ammoniates, J. Phys. Chem. C 116 (2012) 17351–17359.
[100] P.G. Yot, V. Yadav, S.O. Amar, J.-P. Itiè, U.B. Demirci, G. Maurina, Unraveling the mechanical behaviour of hydrazine borane (NH_2-NH_2-BH_3), Phys. Chem. Chem. Phys. 20 (2018) 2845–2850.
[101] R. Moury, G. Moussa, U.B. Demirci, J. Hannauer, S. Bernard, E. Petit, A.V.D. Lee, P. Mielea, Hydrazine borane: synthesis, characterization, and application prospects in chemical hydrogen storage, Phys. Chem. Chem. Phys. 14 (2012) 1768–1777.
[102] H. Wu, W. Zhou, F.E. Pinkerton, T.J. Udovic, T. Yildirimad, J.J. Rush, Metal hydrazinoborane $LiN_2H_3BH_3$ and $LiN_2H_3BH_3$-$2N_2H_4BH_3$: crystal structures and high-extent dehydrogenation, Energy Environ. Sci. 5 (2012) 7531–7535.
[103] R. Moury, U.B. Demirci, T. Ichikawa, Y. Filinchuk, R. Chiriac, A.V.D. Lee, P. Miele, Sodium hydrazinidoborane: a chemical hydrogen-storage material, ChemSusChem 6 (2013) 667–673.
[104] Y.S. Chua, Q. Pei, X. Ju, W. Zhou, T.J. Udovic, G. Wu, Z. Xiong, P. Chen, H. Wu, Alkali metal hydride modification on hydrazine borane for improved dehydrogenation, J. Phys. Chem. C 118 (2014) 11244–11251.
[105] J.G.E. Ricker, Borinhydrazin und seine Pyrolyseprodukte, J. Inorg. General Chem. 310 (1961) 123–142.
[106] S. Mebs, S. Grabowsky, D. Förster, R. Kickbusch, M. Hartl, L.L. Daemen, W. Morgenroth, P. Luger, B. Paulus, D. Lentz, Charge transfer via the dative N–B bond and dihydrogen contacts. Experimental and theoretical electron density studies of small Lewis Acid–Base adducts, J. Phys. Chem. A 114 (2010) 10185–10196.
[107] R. Moury, U.B. Demirci, V. Ban, Y. Filinchuk, T. Ichikawa, L. Zeng, K. Goshome, P. Miele, Lithium hydrazinidoborane: a polymorphic material with potential for chemical hydrogen storage, Chem. Mater. 26 (2014) 3249–3255.
[108] S. Pylypko, J.F. Petit, S. Ould-Amara, N. Hdhili, A. Taihei, R. Chiriac, T. Ichikawa, M. Cretin, P. Miele, U.B. Demirci, Metal hydrideehydrazine borane: towards hydrazinidoboranes or composites as hydrogen carriers, Int. J. Hydrogen Energy 40 (2015) 14875–14884.
[109] A.D. Sutton, A.K. Burrell, D.A. Dixon, E.B. Garner, J.C. Gordon, T. Nakagawa, K.C. Ott, J.P. Robinson, M. Vasiliu, Regeneration of ammonia borane spent fuel by direct reaction with hydrazine and liquid ammonia, Science 331 (2011) 1426–1429.
[110] T. Li, K. Wang, J.G. Zhang, Theoretical study of the structure and dehydrogenation mechanism of sodium hydrazinidoborane, J. Theor. Comput. Chem. 16 (2017) 1750020–1750021, 1750020-13.
[111] L.H. Jepsen, M.B. Ley, Y.S. Lee, Y.W. Cho, M. Dornheim, J.O. Jensen, Y. Filinchuk, J.E. Jørgensen, F. Besenbacher, T.R. Jensen, Boron–nitrogen based hydrides and reactive composites for hydrogen storage, Mater. Today 17 (2014) 129–135.
[112] H.W. Li, S. Orimo, Y. Nakamori, K. Miwa, N. Ohba, S. Towata, A. Züttel, Materials designing of metal borohydrides: viewpoints from thermodynamical stabilities, J. Alloys Compd. 446–447 (2007) 315–318.
[113] M. Zhu, Introduction to Advanced Hydrogen Storage Materials, Science China Press, Beijing, China, 2015.
[114] S.R. Johnson, W.I.F. David, D.M. Royse, M. Sommariva, C.Y. Tang, F.P.A. Fabbiani, M.O. Jones, P.P. Edwards, The monoammoniate of lithium borohydride, $Li(NH_3)BH_4$: an effective ammonia storage compound, Chem. Asian J. 4 (2009) 849–854.
[115] G. Soloveichik, J.H. Her, P.W. Stephens, Y. Gao, J. Rijssenbeek, M. Andrus, J.C. Zhao, Ammine magnesium borohydride complex as a new material for hydrogen storage: structure and properties of $Mg(BH_4)_2{\cdot}2NH_3$, Inorg. Chem. 47 (2008) 4290–4298.
[116] Y. Yang, Y. Liu, Y. Li, M. Gao, H. Pan, Synthesis and thermal decomposition behaviors of magnesium borohydride ammoniates with controllable composition as hydrogen storage materials, Chem. Asian J. 8 (2013) 476–481.
[117] H.L. Chu, G.T. Wu, Z.T. Xiong, J.P. Guo, T. He, P. Chen, Structure and hydrogen storage properties of calcium borohydride diammoniate, Chem. Mater. 22 (2010) 6021–6028.
[118] Z.W. Tang, Y.B. Tan, Q.F. Gu, X.B. Yu, A novel aided-cation strategy to advance the dehydrogenation of calcium borohydride monoammoniate, J. Mater. Chem. 22 (2012) 5312–5318.
[119] L.H. Jepsen, M.B. Ley, R. Cerny, Y.S. Lee, Y.W. Cho, D. Ravnsbæk, F. Besenbacher, J. Skibsted, T.R. Jensen, Trends in syntheses, structures, and properties for three series of ammine rare-earth metal borohydrides, $M(BH_4)_3{\cdot}nNH_3$ (M = Y, Gd, and Dy), Inorg. Chem. 54 (2015) 7402–7414.
[120] F. Yuan, Q.F. Gu, Y. Guo, W.W. Sun, X.W. Chen, X.B. Yu, Structure and hydrogen storage properties of the first rare-earth metal borohydride ammoniate: $Y(BH_4)_3{\cdot}4NH_3$, J. Mater. Chem. 22 (2012) 1061–1069.
[121] F. Yuan, Q.F. Gu, X.W. Chen, Y.B. Tan, Y.H. Guo, X.B. Yu, Complex ammine titanium(III) borohydrides as advanced solid hydrogen-storage materials with favorable dehydrogenation properties, Chem. Mater. 24 (2012) 3370–3379.
[122] L.H. Jepsen, M.B. Ley, Y. Filinchuk, F. Besenbacher, T.R. Jensen, Tailoring the properties of ammine metal borohydrides for solid-state hydrogen storage, ChemSusChem 8 (2015) 1452–1463.
[123] Z. Tang, F. Yuan, Q. Gu, Y. Tan, X. Chen, C.M. Jensen, X. Yu, Scandium and vanadium borohydride ammoniates: enhanced dehydrogenation behavior upon coordinative expansion and establishment of $H^{+\cdots-}H$ interactions, Acta Mater. 61 (2013) 3110–3119.
[124] E. Roedern, T.R. Jensen, Ammine-stabilized transition-metal borohydrides of iron, cobalt, and chromium: synthesis and characterization, Inorg. Chem. 54 (2015) 10477–10482.
[125] Q.F. Gu, L. Gao, Y.H. Guo, Y.B. Tan, Z.W. Tang, K.S. Wallwork, F.W. Zhang, X.B. Yu, Structure and decomposition of zinc borohydride ammonia adduct: towards a pure hydrogen release, Energy Environ. Sci. 5 (2012) 7590–7600.
[126] L.H. Jepsen, Y.S. Lee, R.C. erný, R.S. Sarusie, Y.W. Cho, F. Besenbacher, T.R. Jensen, Ammine calcium and strontium borohydrides: syntheses, structures, and properties, ChemSusChem 8 (2015) 3472–3482.
[127] J.M. Huang, Y.B. Tan, J.H. Su, Q.F. Gu, R. Černý, L.Z. Ouyang, D.L. Sun, X.B. Yu, M. Zhu, Synthesis, structure and dehydrogenation of zirconium borohydride octaammoniate, Chem. Commun. 51 (2015) 2794–2797.
[128] W.W. Sun, X.W. Chen, Q.F. Gu, K.S. Wallwork, Y.B. Tan, Z.W. Tang, X.B. Yu, A new ammine dual-cation (Li, Mg) borohydride: synthesis, structure, and dehydrogenation enhancement, Chem. Eur. J. 18 (2012) 6825–6834.
[129] Y. Yang, Y. Liu, H. Wu, W. Zhou, M. Gao, H. Pan, An ammonia-stabilized mixed-cation borohydride: synthesis, structure and thermal decomposition behavior, Phys. Chem. Chem. Phys. 16 (2014) 135–143.
[130] Y.H. Guo, H. Wu, W. Zhou, X. Yu, Dehydrogenation tuning of ammine borohydrides using double-metal cations, J. Am. Chem. Soc. 133 (2011) 4690–4693.
[131] F. Yuan, X. Chen, Q.F. Gu, Z.W. Tang, X.B. Yu, Synthesis of ammine dual-metal (V, Mg) borohydrides with enhanced dehydrogenation properties, Int. J. Hydrogen Energy 38 (2013) 5322–5329.
[132] Y. Guo, G. Xia, Y. Zhu, L. Gao, X. Yu, Hydrogen release from amminelithium borohydride, $LiBH_4{\cdot}NH_3$, Chem. Commun. 46 (2010) 2599–2601.
[133] X. Zheng, Y. Chua, Z. Xiong, W. Chen, Z. Jiang, G. Wu, P. Chen, The effect of NH_3 content on hydrogen release from $LiBH_4$-NH_3 system, Int. J. Hydrogen Energy 40 (2015) 4573–4578.
[134] Y. Tan, Z. Tang, S. Li, Q. Li, X. Yu, NH_3BH_3/$LiBH_4{\cdot}NH_3$ modified by metal hydrides for advanced dehydrogenation, Int. J. Hydrogen Energy 37 (2012) 18101–18107.
[135] K. Wang, J.G. Zhang, X.Q. Lang, The mechanism of controllable dehydrogenation: CPMD study of $M(BH_4)_x(NH_3)_y$ (M = Li, Mg) decomposition, Phys. Chem. Chem. Phys. 18 (2016) 7015–7019.
[136] G. F. Huff, A. D. McElroy, R. M. Adams, Electrochemical preparation of metal borohydrides. U.S. Patent: 2855353, 1958.
[137] R.W. Parry, G. Kodama, D.R. Schultz, Molecular weight measurements in liquid ammonia. The molecular weights of the methylamine-boranes, the "diammoniate of diborane," ammonia-boron trifluoride and other substances, J. Am. Chem. Soc. 80 (1958) 24–27.
[138] Y. Li, Y. Liu, X. Zhang, D. Zhou, Y. Lu, M. Gao, H. Pan, An ultrasound-assisted

wet-chemistry approach towards uniform $Mg(BH_4)_2$•$6NH_3$ nanoparticles with improved dehydrogenation properties, J. Mater. Chem. A 4 (2016) 8366–8373.
[139] Y. Yang, Y. Liu, Y. Li, M. Gao, H. Pan, Fluorine-substituted $Mg(BH_4)_2$•$2NH_3$ with improved dehydrogenation properties for hydrogen storage, J. Mater. Chem. A 3 (2015) 570–578.
[140] Y. Li, Y. Liu, X. Zhang, Y. Yang, M. Gao, H. Pan, Hydrogen storage properties and mechanisms of a $Mg(BH_4)_2$·$2NH_3$–$NaAlH_4$ combination system, Int. J. Hydrogen Energy 41 (2016) 2788–2796.
[141] X. Chen, F. Yuan, Q. Gu, Y. Tan, H. Liu, S. Dou, X. Yu, Improved dehydrogenation properties of the combined $Mg(BH_4)_2$·$6NH_3$–nNH_3BH_3 system, Int. J. Hydrogen Energy 38 (2013), 16199–16127.
[142] X. Chen, X. Yu, Electronic structure and initial dehydrogenation mechanism of $M(BH_4)_2$·$2NH_3$ (M = Mg, Ca, and Zn): a first-principles investigation, J. Phys. Chem. C 116 (2012) 11900–11906.
[143] X.W. Chen, F. Yuan, Y.B. Tan, Z.W. Tang, X.B. Yu, Improved dehydrogenation properties of $Ca(BH_4)_2$·nNH_3 (n = 1, 2, and 4) combined with $Mg(BH_4)_2$, J. Phys. Chem. C 116 (2012) 21162–21168.
[144] Y. Guo, X. Yu, W. Sun, D. Sun, W. Yang, The hydrogen-enriched Al–B–N system as an advanced solid hydrogen-storage candidate, Angew. Chem. Int. Ed. 50 (2011) 1087–1091.
[145] Y. Tan, Q. Gu, J.A. Kimpton, Q. Li, X. Chen, L. Ouyang, M. Zhu, D. Sun, X. Yu, A synergistic strategy established by the combination of two H-enriched B–N based hydrides towards superior dehydrogenation, J. Mater. Chem. A 1 (2013) 10155–10166.
[146] Y.H. Guo, Y.X. Jiang, G.L. Xia, X.B. Yu, Ammine aluminium borohydrides: an appealing system releasing over 12 wt% pure H_2 under moderate temperature, Chem. Commun. 48 (2012) 4408–4410.
[147] M. Li, F. Yuan, Q. Gu, X. Yu, Synthesis and advanced dehydrogenation properties of niobium-based ammine borohydride, Int. J. Hydrogen Energy 38 (2013) 9236–9242.
[148] K. Wang, Q. Liu, X.Q. Lang, K. Tang, J.G. Zhang, What's the appropriate precondition for ammine metallic borohydrides to generate pure hydrogen? Int. J. Hydrogen Energy 42 (2017) 14936–14941.
[149] Y. Bai, Z. Pei, F. Wu, C. Wu, Role of metal electronegativity in the dehydrogenation thermodynamics and kinetics of composite metal borohydride-$LiNH_2$ hydrogen storage materials, ACS Appl. Mater. Interfaces 10 (2018) 9514–9521.
[150] M. Wang, L. Ouyang, C. Peng, X. Zhu, W. Zhu, H. Shao, M. Zhu, Synthesis and hydrolysis of $NaZn(BH_4)_3$ and its ammoniates, J. Mater. Chem. A 5 (2017) 17012–17020.
[151] M. Li, Q. Gu, X. Li, X. Yu, Dehydrogenation properties of chromium-based ammine borohydrides: $CrCl_3$·nNH_3/$3LiBH_4$ (n = 3, 4 and 5), Int. J. Hydrogen Energy 41 (2016) 733–739.
[152] K. Wang, Q. Liu, X.Q. Lang, K. Tang, J.G. Zhang, What's the appropriate precondition for ammine metallic borohydrides to generate pure hydrogen, Int. J. Hydrogen Energy 42 (2017) 14936–14941.